Redistributive Non-Dissipative Battery Balancing Systems with Isolated DC/DC Converters: Theory, Design, Control and Implementation

REDISTRIBUTIVE NON-DISSIPATIVE BATTERY BALANCING SYSTEMS WITH ISOLATED DC/DC CONVERTERS: THEORY, DESIGN, CONTROL AND IMPLEMENTATION

BY

LUCAS MCCURLIE, B.Tech.

A THESIS

SUBMITTED TO THE DEPARTMENT OF ELECTRICAL & COMPUTER ENGINEERING

AND THE SCHOOL OF GRADUATE STUDIES

OF MCMASTER UNIVERSITY

IN PARTIAL FULFILMENT OF THE REQUIREMENTS

FOR THE DEGREE OF

MASTER OF APPLIED SCIENCE

Master of Applied Science (2016) McMaster University

(Electrical & Computer Engineering) Hamilton, Ontario, Canada

TITLE:	Redistributive Non-Dissipative Battery Balancing Systems with Isolated DC/DC Converters: Theory, Design, Control and Implementation
AUTHOR:	Lucas McCurlie Bachelor of Technology, Process Automation McMaster University, Hamilton, ON, Canada
SUPERVISOR:	Dr. Ali Emadi
NUMBER OF PAGES:	xii, 87

I would like to dedicate this thesis to my parents, John and Carmen McCurlie for encouraging me to follow my dreams and pursue my passions. I would also like to dedicate this to my girlfriend Stacie Wiertel for supporting me through my academic journey and inspiring me to keep moving forward. Lastly, this thesis is dedicated to my brother John William McCurlie. You may not be with us anymore but the memory of you will always be in our hearts.

Abstract

Energy storage systems with many Lithium Ion battery cells per string require sophisticated balancing hardware due to individual cells having manufacturing inconsistencies, different self discharge rates, internal resistances and temperature variations. For capacity maximization, safe operation, and extended lifetime, battery balancing is required. Redistributive non-dissipative balancing further improves the pack capacity and efficiency over a Dissipative approach where energy is wasted as heat across shunt resistors. Redistribution techniques dynamically shuttles charge to and from weak cells during operation such that all of the stored energy in the stack is utilized. This thesis identifies and develops different balancing control methods. These methods include a unconstrained optimization problem using a Linear Quadratic Regulator (LQR) and a constrained optimization problem using Model Predictive Control (MPC). These methods are benchmarked against traditional rule based (RB) balancing. The control systems are developed using MATLAB/Simulink and validated experimentally on a multiple transformer individual cell to stack topology. The implementation uses the DC2100A Demo-board from Linear Technology with bi-directional flyback converters to transfer the energy between the cells.

Acknowledgements

This research was undertaken, in part, thanks to funding from the Canada Excellence Research Chairs Program. I would like to thank my supervisor Dr. Emadi for growing my interest and passion for Electric Vehicles. Dr. Emadi's inspiring words fueled my ambitions and I am truly grateful for his guidance throughout this Masters. My deepest gratitude goes to Dr. Matthias Preindl for co-supervising this thesis research. His teaching ability and motivation consistently challenged my boundaries and pushed me towards my goals. I would also like to thank my friends and colleagues for all of their support and encouragement.

List of abbreviations

Ah	Ampere-hour
BEV	Battery Electric Vehicle
BMS	Battery Management System
C2C	Cell to Cell
C2S	Cell to Stack
CCS	Code Composer Studio
COPM	Constant Operating Point Modulation
DoD	Depth of Discharge
EOL	End of Life
EV	Electric Vehicle
ESS	Energy Storage System
HEV	Hybrid Electric Vehicle
ICE	Internal Combustion Engine
Li-Ion	Lithium Ion
LQR	Linear Quadratic Regulator
MPC	Model Predictive Control
NiMH	Nickelmetal hydride
OCV	Open Circuit Voltage
PHEV	Plug-in Electric Vehicle
PWM	Pulse Width Modulation
RB	Rule Based
S2C	Stack to Cell
SoC	State-of-Charge
SoH	State-of-Health
TMS	Thermal Management System
V	Volts
W	Watt
Wh	Watt-hour

List of symbols

$\widehat{C}$ (Ah)	Maximum Charge Capacity
E_U	Total Initial Unbalanced Energy
E_L	Total Energy Loss
E_A	Final Additional Energy
$\widehat{I}$ (A)	Maximum Link Current
$\widetilde{i}$ (Ah)	Estimated Discharge Current
$\widetilde{i}$ (Ah)	Estimated Charge Current
i_c (A)	Average balancing link current
I_M (A)	Maximum Primary Current
k	High level Sampling Instant
K_{lqr}	LQR Gain
L_p (μH)	Primary Inductance
L_s (μH)	Secondary Inductance
m	Number of links
η_B	Balancing efficiency
n	Number of cells
N_r (2:1)	Flyback Turns Ratio
τ (s)	Time to balance
T_a (s)	Maximum Operational Sampling Time
T_b (s)	Switch On Time
T_p (s)	Low level Controller Sampling Time
T_s (s)	High level Controller Sampling Time
$\bar{u}$	Normalized balancing current
V_c (V)	Cell Voltage
V_s (V)	Stack Voltage
x_0	Initial State-of-charge
x	State-of-charge
x_τ	Balanced State-of-charge

Contents

List of Figures

Chapter 1

Introduction and Problem Statement

1.1 Introduction

Electric Vehicles (EV) have gained significant attention due to elevated atmospheric pollution, a spreading concern for the reliance on fossil fuels as well as harsher government policies on carbon emissions and greenhouse gases. Without any formal change in the policy, the International Energy Agency (IEA) predicts a 70% increase in oil consumption and a 130% increase in CO_2 emissions by 2050, raising the global average temperature by 6°C [9, 10]. Despite this, the sales of alternative fuel vehicles still suffer due to consumer range anxiety, a lack of charging stations, high initial purchase price and longer fueling times all compared to the conventional internal combustion engine (ICE) vehicle [11, 12].

These alternative fuel vehicles include Plug-in Hybrid Electric Vehicles (PHEV), conventional Hybrid Electric Vehicles (HEV) and full Battery Electric Vehicles (BEV).

An umbrella generalization for all Electric Vehicles is represented as xEVs. The main components in any xEV powertrain is the electric motor/generator, the Energy Storage System (ESS) and the power electronics associated with energy conversion and transfer between the electric machine and Storage System [1]. On-board a PHEV and HEV, another powertrain exists to drive the wheels using a gasoline engine with a fuel tank. PHEVs are meant to be plugged into external charging stations that recharges the battery pack. HEVs uses the internal combustion engine and regenerative braking to recharge the battery pack as it drives [1] and has has no plug in capabilities. Examples on the market today of PHEV are Cadillac ELR, Chevrolet Volt and Toyota Prius. Full BEVs use electric power from the batteries to move the vehicle and has no ICE on-board. Examples of full BEVs are Ford Focus Electric, Nissan Leaf and the Tesla Model S. Governments initiatives are using EVs in different ways such as in national parks, school campus patrol and police departments. The United States Army even intends to replace 28000 vehicles with various types of xEVs [13].

However, wide adoption of EVs require improvements in the battery technologies of today [10, 14]. The battery is often viewed as one of the major barriers for mass marketing [10, 14]. There are different ways to improve upon existing battery packs and increase pack capacity. The first method is through different battery chemistries offering larger amounts of energy density. A set of specific goals have been established by the U.S. Advanced Battery Consortium (USABC) to be reached by 2020 for full electric vehicle battery packs. The goals are to have a single cells specific energy reach 350 Wh/kg, a cycle life of 1000 cycles and a cost of $100/kWh at production volumes of 100,000 45 kWh units. These reflect the direction of todays research efforts in battery technology that is to increase specific energy and cycle life yet

reduce cost [10].

Another way to improve battery packs is to increase the size of the pack by adding more cells. The problem with this is that it not only increases the physical space and weight of the vehicle but it will lead to a nearly exponential reduction in the battery life as the number of cells increases [15]. This reduction of battery life is primarily caused by cell imbalances that occur over time due to manufacturing inconsistencies, different self discharge rates, internal resistances and temperature variations. The use of Lithium Ion batteries in EVs has a broad application spectrum such as aircraft e-taxis, hybrid diesel trains, electrified buses and electric vehicles. The reason why Lithium Ion cells are typically used is because they have high energy density, low self-discharge rates and high cell voltages.

A Battery Management System (BMS) is implemented to avoid the harmful effects of cell imbalances, improve the effective capacity of the pack and keep each cell within a predefined operational safety region. A balancing system is used within the BMS to keep each cells state-of-charge balanced (equal). The two types of balancing systems are categorized as either *Dissipative* or *Non-Dissipative*. The Dissipative balancing approach draws excess energy from strong cells then dissipate this energy as heat through external shunt resistors [16, 17]. This method, although inexpensive is wasteful of energy that can be re-purposed elsewhere. The Non-dissipative redistributive technique shuttles the excess energy from the strong cells into the weak ones using power electronics [5, 18, 19]. Three approaches of achieving redistributive balancing are cell to cell (C2C), cell to stack (C2S) and stack to cell (S2C). A C2C approach transfers the excess energy between adjoining cells. A C2S approach transfers the excess energy from strong cells then redistributes it back onto the battery

stack. Likewise, a S2C approach transfers the excess energy from the battery stack to the weak cells. It is possible to achieve simultaneously charge and discharge of individual cells by integrating a S2C with C2S.

Each method can use different types of strategies to control the battery currents for individual cells. In this thesis, a redistributive non-dissipative battery balancing system is developed using flyback converters for shuttling the energy simultaneous to and from each cell in the pack. Different control strategies are implemented on top of the hardware to compare performance variation and to help understand better balancing practices. Furthermore, a model predictive control technique is developed using performance metrics from [5], which balances the cells in minimum time. A minimum time to balance control can be used in electric fleet vehicles where time to balance is important. Other applications for redistributive control are further explored.

1.2 Research problem definition

Electric fleet vehicles are becoming more common as companies are starting to realize the advantage of lower operating and maintenance costs [13]. Medium and heavy duty Battery Electric Vehicles and Plug-In Hybrids have begun penetrating several transportation sectors such as transit buses and delivery vehicles. Benefits in these sectors are reduced road traffic noise, less noise polluted cities and more sustainable transportation. Further improvements over ICEs are due to a reduction in maintenance cost (as brakes do not wear as easily due to regenerative braking), fewer engine fluids and fewer moving parts [20]. By 2020, Fort Motor Company believes that 10% to 25% of its global fleet will be electrified. Purolator is purchasing more electric

vehicles for delivery application; Ford and Frieghtliner will be selling full BEV utility vehicles soon and Navistar intends to produce EVs as well [13].

Lithium Ion batteries require balancing due to individual cells having manufacturing inconsistencies, different self discharge rates, internal resistances and temperature variations. The desired result of this research is to present a Non-dissipative redistributive balancing system to further improve on the pack capacity and balancing efficiency over a active dissipative approach being deployed in most EVs. As batteries are charged and discharges in a vehicle, they degrade over time. Car manufactures typically define the end-of-life (EOL) as 20% reduction in the battery capacity from when it was first installed into the car. This degradation also increases the resistance and reduces the amount of power the battery is able to deliver. However, once a cell reaches this 20% reduction in battery capacity does not mean it cannot be used for another purpose.

Two applications where redistributive non-dissipative balancing may be useful in the future are in delivery fleet vehicles and second life battery applications. Delivery fleet vehicles might find it useful to have a minimum time to balance implementation since this could mean more time on the road. Battery second life applications use recycled battery packs for stationary power systems with mismatched capacities and large initial imbalances. Having optimization methods embedded in the balancing, could mean weak capacity cells would not hinder the system.

1.3 Research goals and requirements

Different control approaches are simulated using Matlab Simulink and are compared to experimental results conducted on a small test bench lab setup. The three control

approaches being compared are Rule Based (RB), Linear Quadratic Regulator (LQR) and Model Predictive Control (MPC). Results show that MPC and LQR achieve a single point convergence of the state-of-charge when compared against a common Rule Based algorithm. However, LQR balances in less time due to saturation of the balancing currents. RB and MPC balance in the same time but MPC has a higher balancing efficiency.

In this thesis, a new performance metric is introduced for battery balancing. The balancing hardware and control strategy have a associated balancing efficiency (η_B). This balancing efficiency is attributed to the total amount of initial unbalanced energy and the total amount of lost energy during balancing the cells. This metric is used to compare RB control and the MPC as both provide nearly optimal minimum time to balance but MPC has higher balancing efficient. It is also used to show that active dissipative approach has a balancing efficiency of zero due to all the unbalanced energy being lost as heat to the resistors.

1.4 Electric Vehicle Battery Technologies

A battery contains a number of electrically connected cells that convert stored chemical energy into electric energy. Each cell is a combination of two electrodes arranged so that an overall oxidation-reduction reaction produces an electromotive force. There exists several types of batteries, all with different applications. A primary battery is one that is disposable and cannot be recharged. It has irreversible chemical reactions inside the electrode to generate electricity. In the attempt to recharge this type of battery, it would produce hazardous liquids that would eventually leak. For an example, a Alkaline Manganese cell known as the common household battery is often

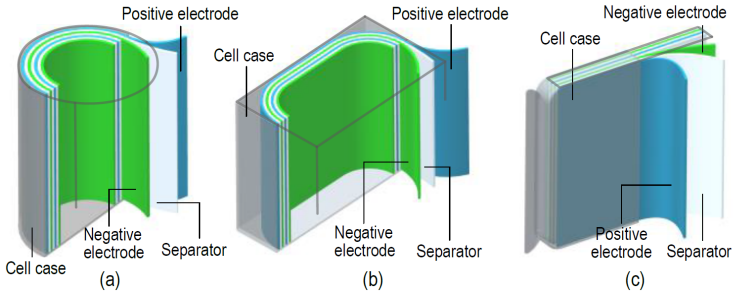

Figure 1.1: Basic Battery Illustration [1].

found in smoke alarms and Television remotes.

A secondary battery is one that involves a reversible chemical reaction and can be recharged multiple times. This type of battery is used in Electric Vehicles for obvious reasons but can also be found in ICEs as Lead-acid batteries for starting the car. The components of a secondary battery consist of a anode, cathode, separators, current collector and electrolyte. The anode is the negative electrode and is where the electrons are generated. The cathode is the positive electrode and is where the electrons return after doing work outside of the battery. The separator is the insulating divider and is physically separated by the two electrodes. It helps move the ions from one electrode to the other and also prevents any electrons from crossing over. The current collector is placed on each of the electrodes and its primary function is to conduct electrons to and from the external electrical circuit. The final component is the electrolyte. This facilitates ions that are essential to support the electrochemical reactions.

Due to its superior performance, Lithium ion batteries are leading the EV market over Lead acid batteries and NiMH batteries [10, 21, 22]. For this reason, it will be used as the main focus for this thesis. The anode (negative electrode) is made of carbon and the cathode (positive electrode) consists of a metal oxide. The charging

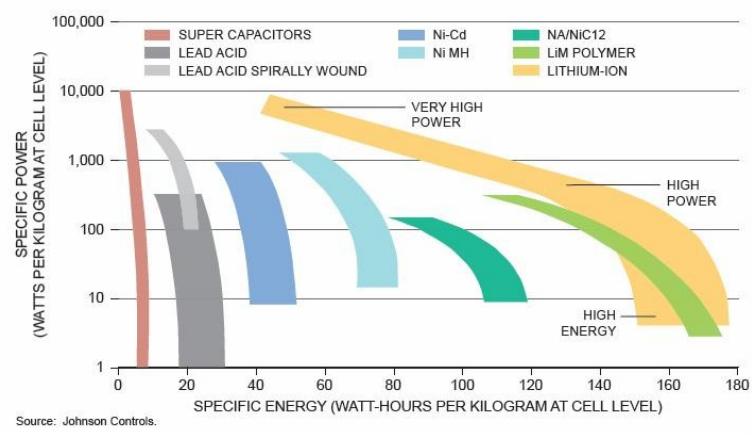

Figure 1.2: Ragone Plot of Battery Chemistries.

and discharging of the cell occurs by transferring Lithium ions between these two electrodes across the solution and electrons through the current collectors. The separator will inhibit the flow of electrons but conduct ions. Fig. 1.1 shows different cell formats such (a) small cylindrical cell, (b) prismatic cell and (c) pouch cell. Each format has an appropriate application and is up to the engineer to decide what works best. A more detailed comparison between the different formats can be found in [4].

Lithium Ion batteries typically have a flat discharge curve that associates cell capacity (Ah) to the cells open circuit voltage (OCV). Different curves for different c-rates are provided by many battery manufacturing companies and can be shown in Fig. 1.4. The advantage of having a flat discharge curve is that it simplifies the

Table 1.1: Chemistry Comparison and Summary [23]

Cathode	$LiCoO_2$	$LiMnO_4$	$LiFePO_4$	Polymer
Energy Density (Wh/Kg)	120 - 190	110 - 120	90 - 110	130 - 200
Nominal Voltage (V)	3.6	3.8	3.3	3.7
Discharge Rate	2C/4C	10C/20C	35C/60C	1.5C/3C
Products	Tesla	Nissan	Chrysler	Hyundai

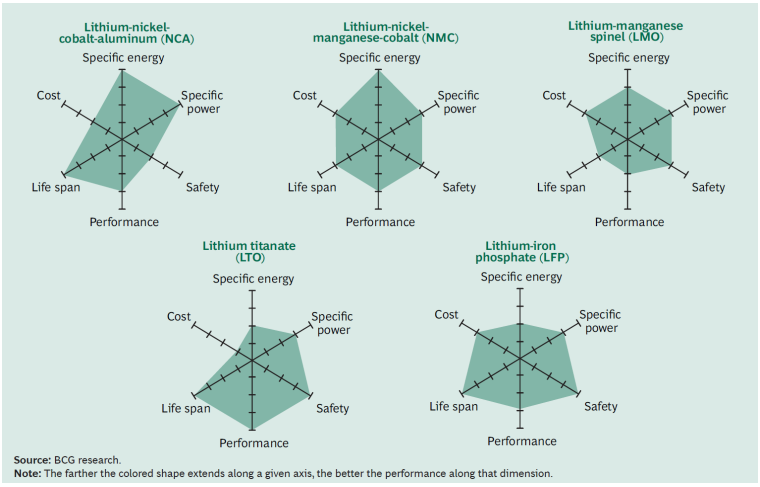

Figure 1.3: Trade offs Among Lithium Ion Battery Technology [2].

design since the supply voltage stays relatively constant throughout discharge cycle. However, it presents a bigger challenge when estimating the batteries SoC since a small deviation in voltage results in a large capacity change. The ragone plot in Fig. 1.2 compares various electrochemical devices. Ultra capacitors are shown to have a high power density but a limited storage capacity thus making them great candidates for capturing regenerative braking energy in electrified vehicles. Fuel cells have a higher energy density but lower power density which limits their applications in Electric Vehicles. Lithium batteries are central to the two and provide the best qualities of both. Fig. 1.3 shows the trade offs among Lithium ion battery types.

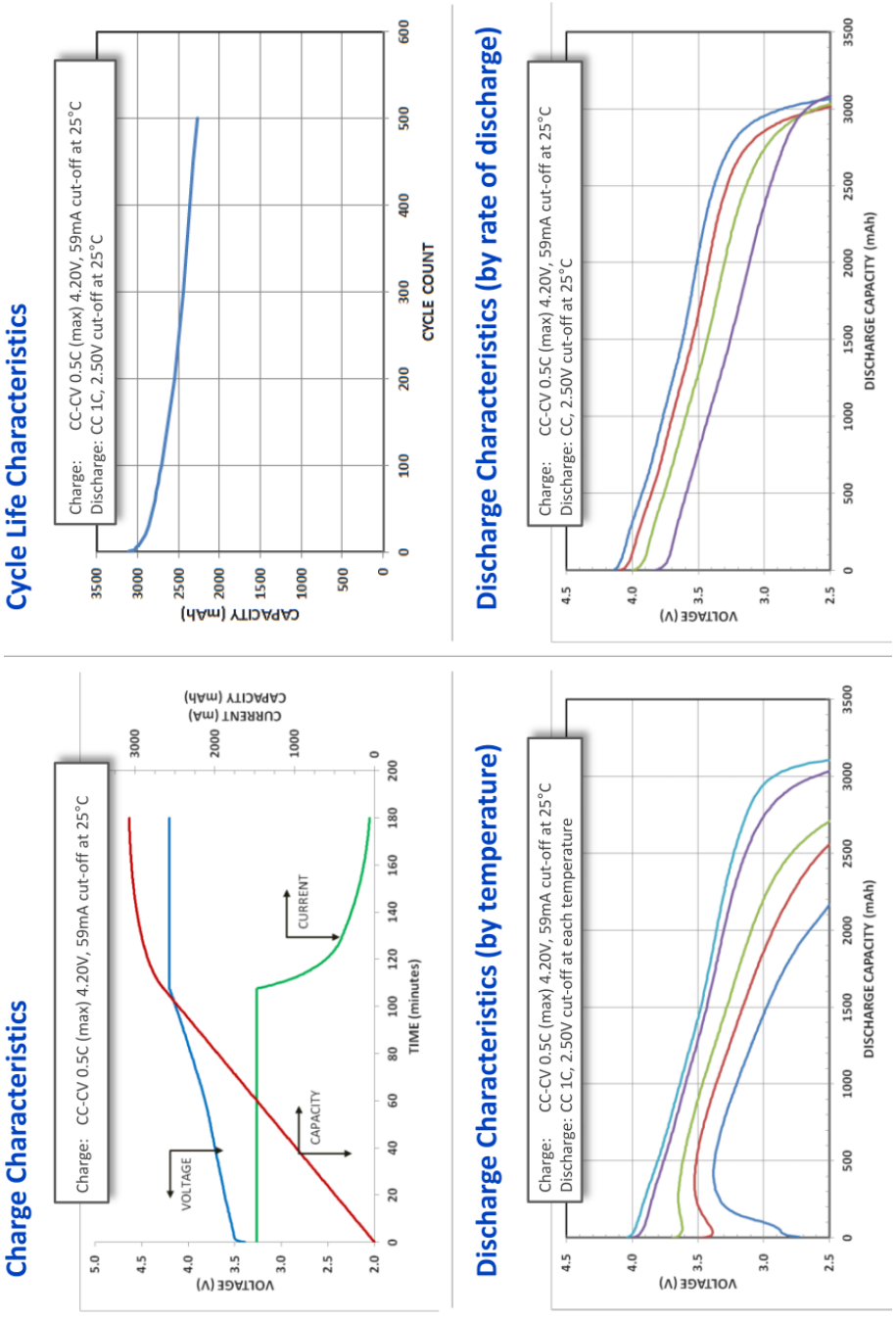

Figure 1.4: Panasonic 18650 cell characteristics [3].

1.5 Basic Battery Terms

In order to fully describe the state and properties of different battery cells, commonly used terms are summarized in the following as a quick reference.

Cell, module, pack. A single cell has two electrodes, separator and electrolyte. A module is a few cells in series or parallel with one another. The battery pack is comprised of many modules to accommodate high voltages and large capacities. For example, the Chevrolet Volt uses 96 Lithium Ion cells in its pack construction.

State-of-Charge (SoC). SoC is an expression that indicates the amount of battery capacity as a percentage of the maximum capacity. The state of charge x is not measurable but can be estimated according to $y = C(x)$ where y is the voltage associated with the battery terminals and C is some nonlinear mapping [24]. Advanced methods for SoC estimation are Kalman filters [25], neural networks [26], electrochemical impedance spectroscopy [27] and fuzzy logic [28, 29]. If Ah capacity is used, the change of SoC can be expressed as

$$\Delta SoC = SoC(t) - SoC(t_0) = \frac{1}{\text{Ah Capacity}} \int_{t0}^{t} u(t)dt \tag{1.1}$$

State-of-Health (SoH). SoH is a ratio of the maximum charge capacity of an aged battery to the maximum charge capacity when the battery was new. It can be expressed as

$$SoH = \frac{\text{Aged Energy Capacity}}{\text{Nomincal Energy Capacity}} \tag{1.2}$$

Terminal Cell voltage (V). Terminal voltage (V_t) is measured between the battery terminals with a load being applied. This changes with state-of-charge and applied current.

Open circuit voltage (V). The voltage that is measured between the battery terminals when no load is applied.

Capacity (Ah). The capacity of a battery is the amount of current it can provide for a certain amount of time. It is typically expressed in Amphours. For example, the Panasonic 18650 cells shown in Fig. 1.4 has a nominal capacity of 3.07 Ah.

C-rate. Typically used when describing how much current a type of battery cell can discharge. A C-rate is a measure of the rate at which a battery can discharge relative to its maximum capacity. A 1C rate means that the discharge current will discharge the entire battery in 1 hour. For a battery with a capacity of 50 Amphours, this equates to a discharge current of 50 Amps. A 5C rate for this battery would be 250 Amps, and a C/2 rate would be 25 Amps.

Cycle Life. Cycle life is the number of discharge-charge cycles before a battery fails to meet specific performance criteria. Under specific charge and discharge conditions, Cycle life can be estimated. The operating life is affected by the rate and depth of cycles as well as temperature and humidity.

Internal resistance. Internal Resistance is the resistance within the battery. In general, it is dependent on the cells state-of-charge and if its being charged or discharged. The batteries efficiency decreases as the internal resistance increases.

Depth of Discharge (DoD). The percentage of battery capacity that has been discharged expressed as a percentage of maximum capacity.

$$DoD = 1 - SoC \tag{1.3}$$

Stored Energy (Wh). The energy stored in a battery depends on its voltage and capacity. A unit of Watthour is typically used.

$$\text{Stored energy (Wh)} = \text{Voltage (V) x Capacity (Ah)} \tag{1.4}$$

Specific energy. Specific energy is the quantity of energy stored in the battery for every kilogram of mass. The specific energy is typically given in Wh/Kg.

$$\text{Specific Energy} = \frac{\text{Stored Energy (Wh)}}{\text{Battery Mass (Kg)}} \tag{1.5}$$

Specific power. Specific power is the amount of power obtained for each kilogram of the battery and is measured in W/Kg.

$$\text{Specific Power} = \frac{\text{Peak Power (W)}}{\text{Battery Mass (Kg)}} \tag{1.6}$$

Thermal management System. TMS protects the battery pack from overheating. This can help extend the packs calender life. EVs which use NiMH batteries use

simple forced air cooling TMS, but more sophisticated and powerful liquid cooling is required for Lithium ion batteries in EV Applications [30].

1.6 Battery Management System (BMS)

The Battery Management System (BMS) is a system used for the following tasks:

1. Monitoring
2. Protection
3. Estimation
4. Control

These four main functions are found in any BMS to ensure safe operation, high performance and longer lifetime expectancy [31, 32]. Protection of Lithium-ion batteries experiencing over and under voltages is essential to maximizing the health and safety of the cells [33]. If over voltage occurs, production of CO_2, C_2H_4 and other gases will increase the internal temperature and pressure causing severe battery damage or an explosion [32]. If under voltage occurs, internal reactions cause the cell to lose a large part of its capacity. The voltage of a battery cell is related to its remaining energy (state-of-charge). Therefore, a weak cell is defined as one that has a lower SoC than the others in the pack. Likewise a strong cell is one that has a higher SoC. Without a on-board balancing system, the cells capacities would drift apart causing weak cells to dominate discharging time and strong cells to dominate charging time. A Battery Management System (BMS) is implemented to avoid the harmful effects of cell imbalances, improve the effective capacity of the pack and keep each cell within

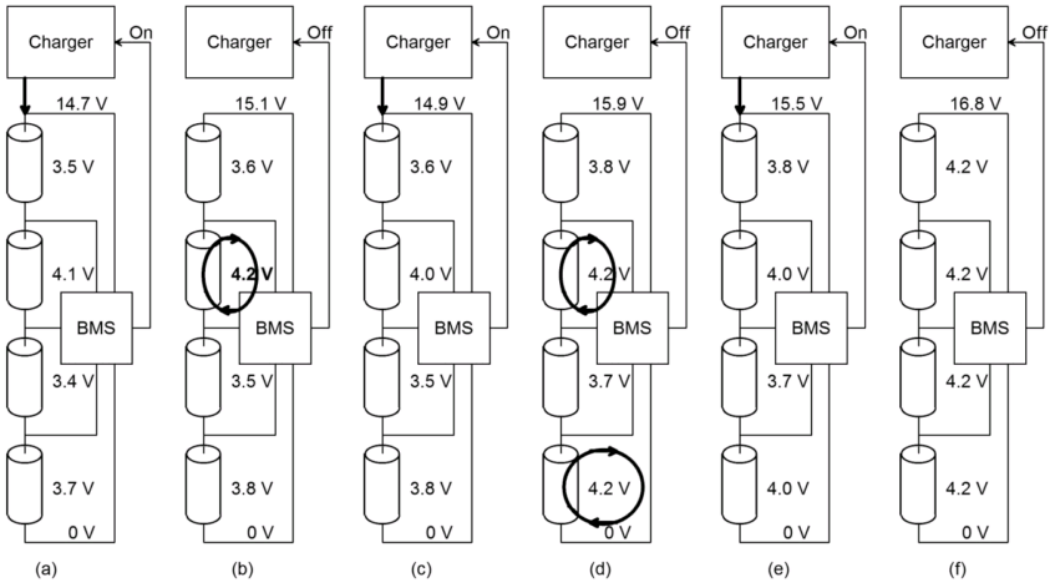

Figure 1.16 Charging with a balancing BMS controlling the charger: (a) charging; (b) charging stops when any one cell reaches the top cutoff voltage; (c) charging restarts after that cell's voltage is slightly reduced by balancing; and (d) the process repeats until (e, f) the pack is balanced.

Figure 1.5: Example Balancing Strategy [4].

a predefined operational safety region. Fig. 1.5 shows a high level conceptual view of voltage based battery balancing.

1.7 Thesis outline

This thesis is organized as follows: Balancing methods including balancing hardware topologies are described in Chapter 2. The power electronics used for redistributive non-dissipative battery balancing are explained in Chapter 3. Development and analysis of different control techniques are presented in Chapter 4. The implementation details for an experimental test bench are described in Chapter 5. Then in Chapter 6, a comparison between all control methods is conducted and discussed. Finally, conclusion remarks are at the end of this thesis in Chapter 7.

Chapter 2

Balancing methods

Electric Vehicles are rapidly shifting towards drivetrains with high-power electric machines and inverters. The battery system therefore needs to be high voltage, high efficiency and have long lifetime [22, 34–36]. The battery cells are connected in series to achieve high voltage levels which will lead to a nearly exponential reduction in the battery life as the number of cells increases [15]. A significant reason for reduced lifetime is charge imbalances of the cells which only degrades even further with time. Cell imbalances arise due to internal effects such as manufacturing inconsistencies, different self-discharge rates and internal resistance as well as external effects such as temperature variations. To avoid damages, correct any imbalances and improve the effective capacity of the pack, an energy balancing system is required [37].

The two types of battery balancing hardware is *dissipative* and *non-dissipative*. A dissipative approach draws excess charge from the cells with a higher state-of-charge and dissipates it through resistors. A non-dissipative approach uses power electronics to transfer excess charge between cells [5, 18, 19, 38]. *Balancing* simply means equalizing all cells state-of-charge in a series connected string. If a unbalanced

string remains as such, the effective capacity of the pack is low. As mentioned before, Lithium Ion battery cells are typically used in EVs because of their superior energy density, self discharge rate and cycle life. However, Li-ion cells have more safety precautions than lead-acid and NiMH [4]. This means while discharging the stack, operation must halt once the weakest cell is completely empty, even if the stronger cells still contain energy. *Redistribution* is defined as dynamically shuttling charge to the weak cells from the stronger cells *during operation* such that all of the stored energy in the stack can be utilized [10, 39].

Redistributive techniques and various hardware topologies have been studied and applied in industry [18] [19] [5]. Three approaches of achieving redistributive balancing are cell to cell (C2C), cell to stack (C2S) and stack to cell (S2C). A *C2C* approach transfers the excess energy between adjoining cells. A *C2S* approach transfers the excess energy from strong cells then redistributes it back onto the battery stack. Likewise, a *S2C* approach transfers the excess energy from the battery stack to the weak cells. By Combining the last two methods, it is possible to simultaneously charge and discharge individual cells. Both classifications can further be divided into *passive* balancing and *active* balancing. Passive balancing relies on system properties and does not require a controller. Faster balancing can be achieved using active balancing systems which use a high level controller to direct the charge and discharge currents per cell.

2.1 Dissipative balancing topologies

A true passive dissipative balancing topology is shown in Fig. 2.1. This topology permanently connects shunt resistors in parallel to each cell during balancing. The way in which this balances is that the cells with the higher voltage will discharge more than the lower voltages. True passive dissipative balancing removes charge from all the cells state-of-charge. This method for balancing can only be used with Lead-acid and NiMH type batteries because these types of cells can be overcharged without severe consequences [19,38]. However, this requires a much larger amount of balancing time. By combining the same topology with a control method and additional hardware i.e switches, a active dissipative balancing topology is formed.

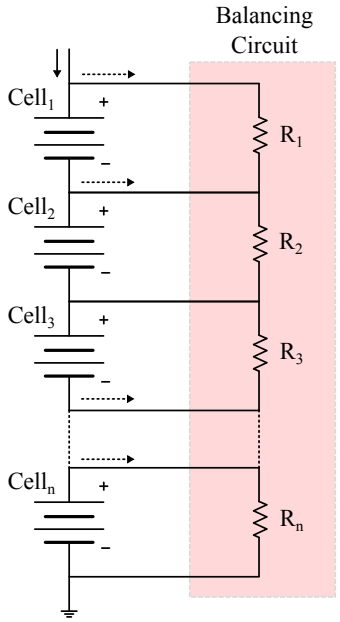

Figure 2.1: Passive Dissipative Balancing using Resisters.

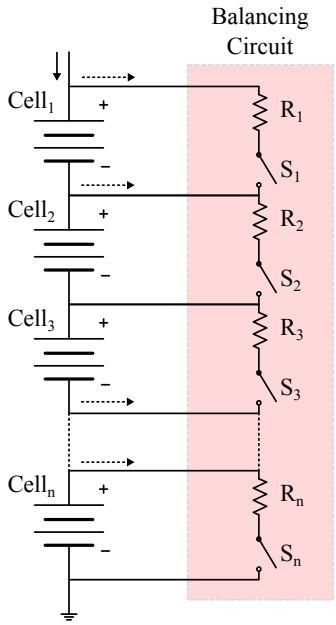

Figure 2.2: Active Dissipative Balancing using Switched Resistors.

Most balancing schemes being used today by Car Manufacturers and other vendors are *unidirectional active dissipative balancers*. This method operates by switching a path from the battery to a parallel resistor for cells with higher voltages. No charge is recovered and the energy is essentially wasted as heat through the resistive element. The time for balancing is reduced when compared with its passive counterpart, but still remains high due to small bleeding currents ($\approx$ 20mA). The switched resistor method for active dissipated balancing is shown in Fig. 2.2. As a side note, resistor values are typically chosen such that the current is small or less than 10mA/Ahr capacity. This translates into each cell roughly being balanced at a rate of 1% per hour [38]. However, if this technique was used during the full operational cycle of the battery (not just charging), it would drain the entire pack in just a few days [38].

2.2 Non-Dissipative balancing topologies

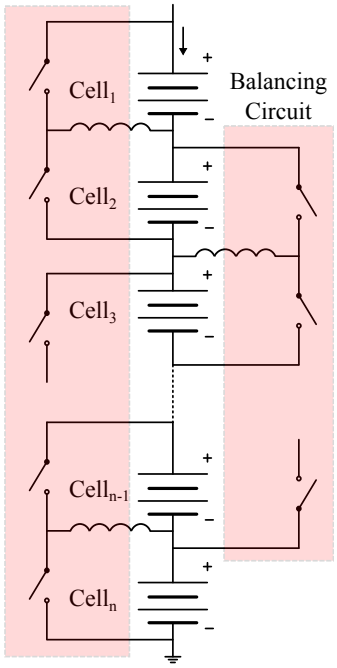

Figure 2.3: Non-dissipative (Shunting) Current Divider.

The general idea behind *non-dissipative active balancing* is using external circuits to transfer energy among the cells in order to balance them. The word *active* will be dropped for simplicity, as all non-dissipative topologies discussed in this thesis are active. The three major categories for non-dissipative balancing are *shunting*, *shuttling* and *energy converters*. Different circuit topologies lead to the three categories. Shunting methods remove excess energy from neighboring cells to make higher voltage cells wait for the lower voltage cells to catch up. This is similar to the active dissipative method but the energy is captured and put back onto the cells instead of being wasted. For example, a shunt topology known as a current divider from [40] is shown in Fig. 2.3. More topologies of similar nature are PWM Controlled Shunting,

Resonant Converter, Boost Shunting and Complete Shunting [19, 38].

The second class of non-dissipative balancing are *shuttling* techniques. These methods utilize external energy storage devices (capacitors and inductors) to shuttle the energy amongst the cells in order to balance them. The three main shuttling topologies are switched capacitor (SC), single switched capacitor (SSC) and double tiered switched capacitor (DTSC) [41]. A single switched capacitor topology is shown in Fig. 2.4. This topology uses a capacitor to store energy and move it between several series connected cells.

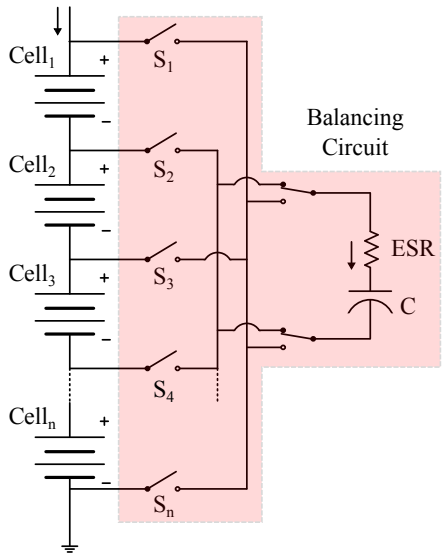

Figure 2.4: Non-dissipative (Shuttling) Single Switched Capacitor.

The final class of cell balancing are grouped together as energy converter topologies. The converters all require isolation such that the input and output side have isolated grounds. These are often referred to as cell to stack topologies as the charge is removed from one cell then distributed equally among all the cells in the stack [5].

Charge can also be drawn equally from all the cells then added to a single cell using bi-directional dc-dc converters. Many topologies exist such as stepup converter, multi-winding transformer, ramp converter, multiple transformers, switched transformer found in [19, 38, 41]. A shared transformer topology is shown in Fig. 2.5.

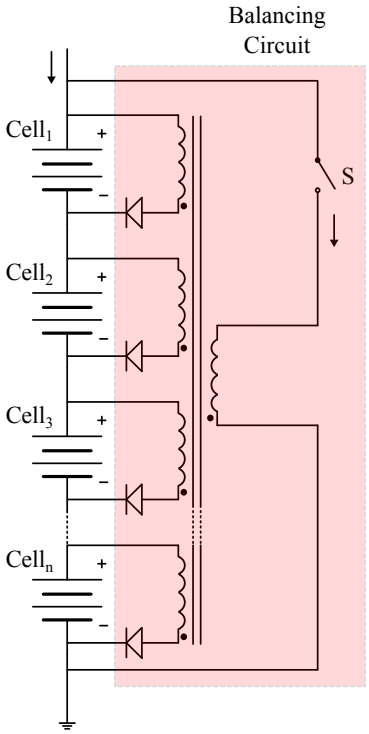

Figure 2.5: Non-dissipative (Energy Converter) shared transformer.

In [5], two performance metrics are defined for evaluating the performance of seven different balancing hardware topologies shown in Fig. 2.6. The two metrics that are defined and analyzed are time required to balanced and energy dissipated during balancing. The results from [5] are shown in Fig. 2.7. Shunting topologies have time to balance that grows linearly with the number of cells and the energy dissipated to balance grows exponentially with the number of cells. Shunting topologies therefore have poor time to balance and energy dissipation. Converter based topologies, more

specifically the individual cell to stack topology shows time to balance and energy dissipated as constant and independent of the number of cells. For this reason, the main focus of this thesis is on the individual cell to stack topology i.e a multiple transformer topology that uses bi-directional flyback converters to realize the battery balancing currents.

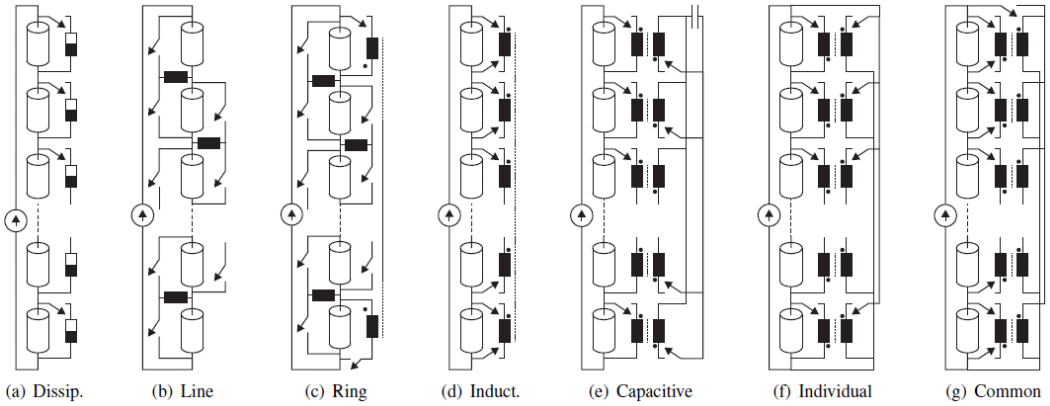

Dissipative (a); Line shunting (b); Ring shunting (c); Inductive storage element (d); Capacitive storage element (e); individual cell to stack (f); Common cell to stack (g)

Figure 2.6: Balance Hardware Topologies from [5].

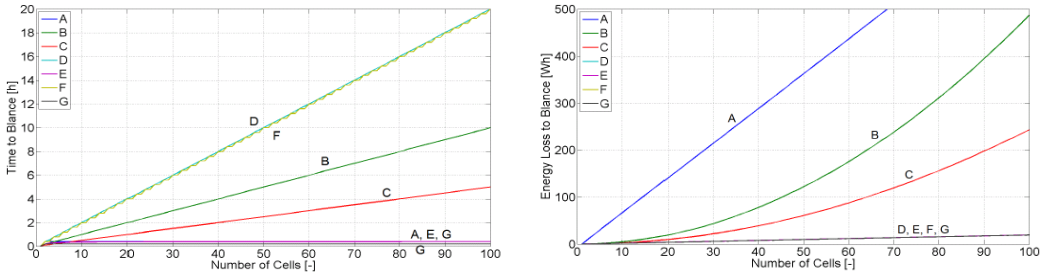

(a) Time to balance $\tau^*(\mathcal{D})$ (b) Energy-loss-to-balance $\varepsilon^*(\mathcal{D})$

A - Dissipative, B - Line shunting, C - Ring shunting, D - Inductive storage element, E - Capacitive storage element, F - Common cell to stack, **G - individual cell to stack**

Figure 2.7: Performance metrics; T2B (a), E2B (b) [5].

Chapter 3

Power Electronics used for Redistributive Battery Balancing

3.1 Overview of Power Electronics

Power electronics is a way of controlling and converting electric power. More specifically, it is the study of switching electronic circuits for the purpose of controlling energy flow. Different classifications are made depending on the type of input and output power requirements. A rectifier converts alternating current (AC) to direct current (DC) and is found in many consumer products such as Televisions and Personal computers. Contrast to the rectifier is a power inverter which converts DC to AC. System design includes parameters such as input voltage, output voltage, frequency and power requirements. Many inverter applications exist such as the use in solar panels. A AC-to-AC converter is one that converts a AC line input to AC inverter output. A very common example of this is used in Variable frequency drives found in electro-mechanical drive systems to control AC motor speed and torque.

3.2 DC-to-DC Converters

The final class in power electronics is DC-to-DC converters which convert one DC voltage level to another. The power levels can range from very low such as in small battery applications, to very high such as in high-voltage power transmission. Low power level applications can be found in cell phones and laptop computers (5 - 10V). High power level applications are Electric vehicles(300V+). In many electrical devices, a large number of sub-circuits exist that require different voltage levels. Instead of using many batteries with different input voltages, a single source is typically used in conjunction with switched DC-to-DC converters to either increase or decrease the voltage levels for their sub-circuits. Many different DC-to-DC Converts exist but the general form is shown Fig. 3.1.

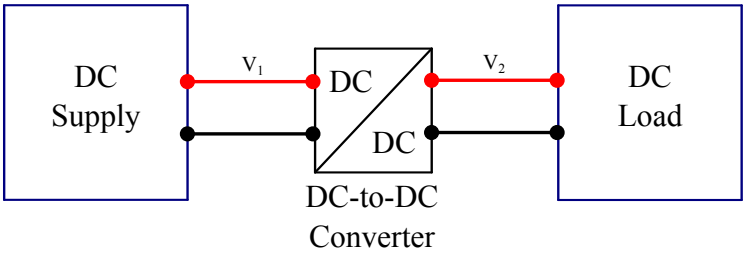

Figure 3.1: General form DC-to-DC Converter.

3.2.1 Buck-boost converter

The buck-boost converter shown in Fig. 3.2a, is a common type of DC-to-DC converter that can either have a output voltage greater than or less than the input voltage. This converter combines a buck (step-down) converter with a boost (step-up) converter. The magnitude of the output voltage is based on the duty ratio of the switching

device. The main components in the buck-boost converter is a power metal-oxide semiconductor field-effect transistor (MOSFET) S, a diode D and an inductor L. For simplicity, the MOSFET is represented by an ideal switch in Fig. 3.2. The basic principle of the buck-boost has two main topological operational states. The first state, shown in Fig. 3.2b.1, is when the MOSFET S is closed. The voltage across the inductor L becomes the input voltage E. The inductor current ramps up at a rate that is proportional to E. The accumulating energy in the inductor is

$$V_L = E = L\frac{di_L}{dt} \tag{3.1}$$

The second state, shown in Fig. 3.2b.2, is when the MOSFET S is open. The diode D is forward-biased and the inductor current ramps down at a rate proportional to E_o. The Energy is transfered from the inductor to the load. For steady-state operation, the difference in the inductor current must be zero over period T as:

$$(\Delta i_L)_{open} + (\Delta i_L)_{closed} = 0 \tag{3.2}$$

$$\frac{Et_c}{L} + \frac{E_o t_a}{L} = 0 \tag{3.3}$$

Thus the voltage conversion ratio of the inverting buck-boost in CCM is expressed as

$$\frac{E_o}{E} = -\frac{D}{1-D} \tag{3.4}$$

where $D = \frac{t_c}{T}$ shown in Fig. 3.3. The magnitude (3.4) of the output voltage is either higher (if $D > 0.5$) or lower (if $D < 0.5$) than the input voltage. Fig. 3.3 shows typical voltage and current waveforms in continuous conduction mode (CCM).

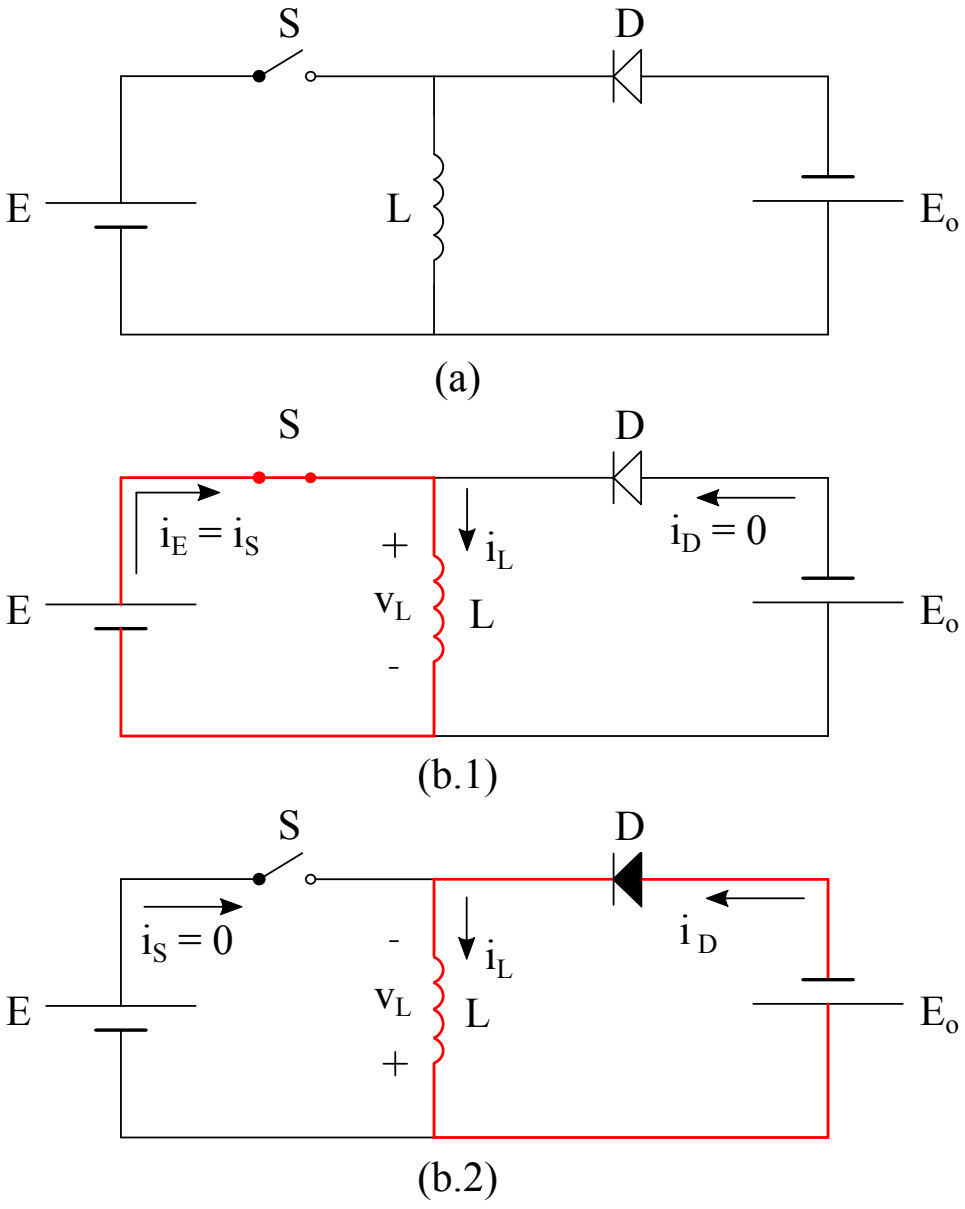

Figure 3.2: Buck-Boost Converter.

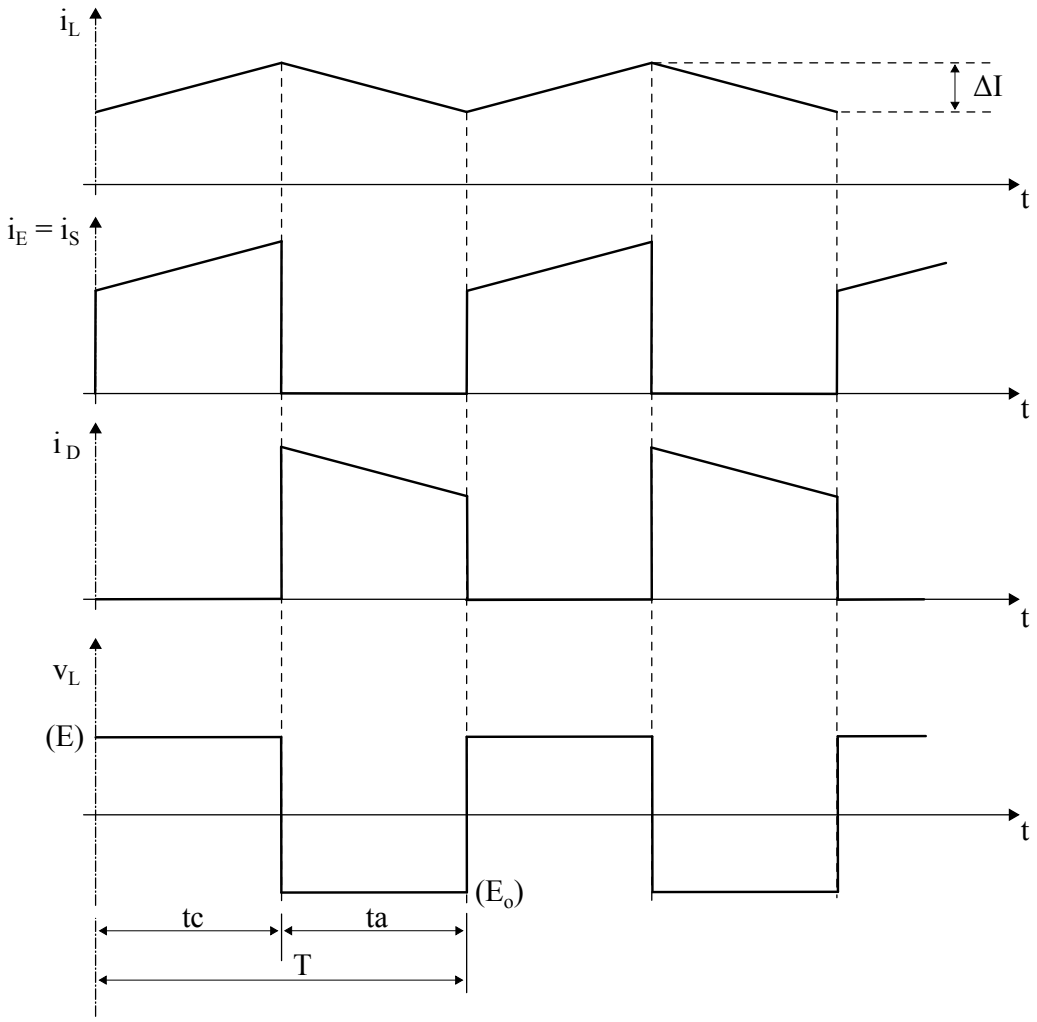

Figure 3.3: Buck-Boost Converter Waveforms (CCM).

3.2.2 Flyback converter

To achieve galvanic isolation, safety, and enhanced noise immunity, the secondary side is electrically isolated from the primary side in a isolated DC/DC converter. This isolation is typically used in EVs to keep the power rating of the switches low [5]. The Flyback converter provides a simple implementation for the redistributive non-dissipated balancing system and has similar inter workings as the buck-boost converter.

The Flyback is commonly used at 50-100W power range but still functions as high voltage power supplies for televisions and computer monitors. Its main advantage is in a low number of components [42] when compared to other isolated topologies. These converter can operate in either Continuous Conduction Mode (CCM) or Discontinuous Conduction Mode (DCM). For the multiple transformer topology in the redistributive non-dissipative balancer, they will be operated in Discontinuous Conduction Mode (DCM) because it requires a smaller transformer, reducing system costs than its Continuous Conduction Mode (CCM) counterpart [6]. Additional voltage on the primary side transformer may be viewed due to ringing associated with the transformer leakage inductance. A snubber circuit is typically required to clamp the magnitude of this ringing voltage to a safe level that is within the peak voltage rating of the transistor [42].

The Flyback converter shown in Fig. 3.5a, is derived from the buck-boost shown in Fig. 3.2a. The main components in the flyback converter is a MOSFET S, a diode D and a isolated transformer that can be modeled by an ideal transformer in parallel with a magnetizing inductance [42]. Again, for simplicity, the MOSFET is represented by an ideal switch in Fig. 3.5. The basic principle of the flyback has two

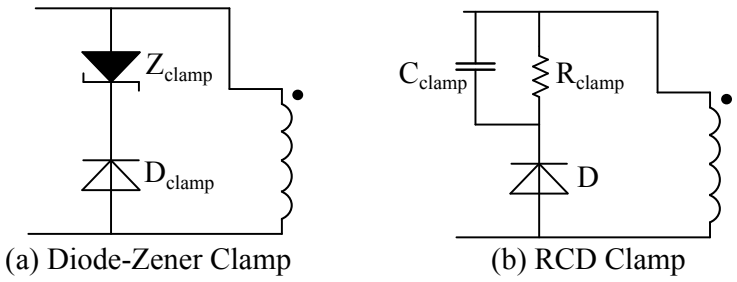

Figure 3.4: Voltage Clamping [6].

main topological operational states. The first state, shown in Fig. 3.2b.1, when the primary switch is closed S, the diode D is reverse biased due to the winding polarities and the inductor voltage $V_1 = E$. The transformer (main inductance) stores energy during this on-time of the MOSFET. The current during the on-time of the primary switch is

$$L_p \frac{di}{dt} = V_1 = E \Rightarrow \frac{I_{M1}}{DT} = \frac{E}{L_p}, \tag{3.5}$$

where D is the duty cycle, T switching period, $V_1 = E$ is the cells voltage for battery balancing and V_o is the stack voltage. The second state, shown in Fig. 3.2b.2, is when the primary switch is opened. In DCM, all the energy stored in the core of the transformer is transfered to the secondary winding, forward biasing the diode and supplying the load. Fig. 3.6 shows the typical voltage and current waveforms in Discontinuous Conduction mode (DCM).

In practice, during the off time of the MOSFET, a high voltage spike due to the transformers leakage inductance can occur. This high voltage spike can cause serious damage to the MOSFET. Therefore, a snubber circuit is used in the Flyback converter to clamp any voltage spike to a safe level. Two clamping circuits are shown in Fig. 3.4. For bi-directional power flow, a second MOSFET replaces the secondary diode.

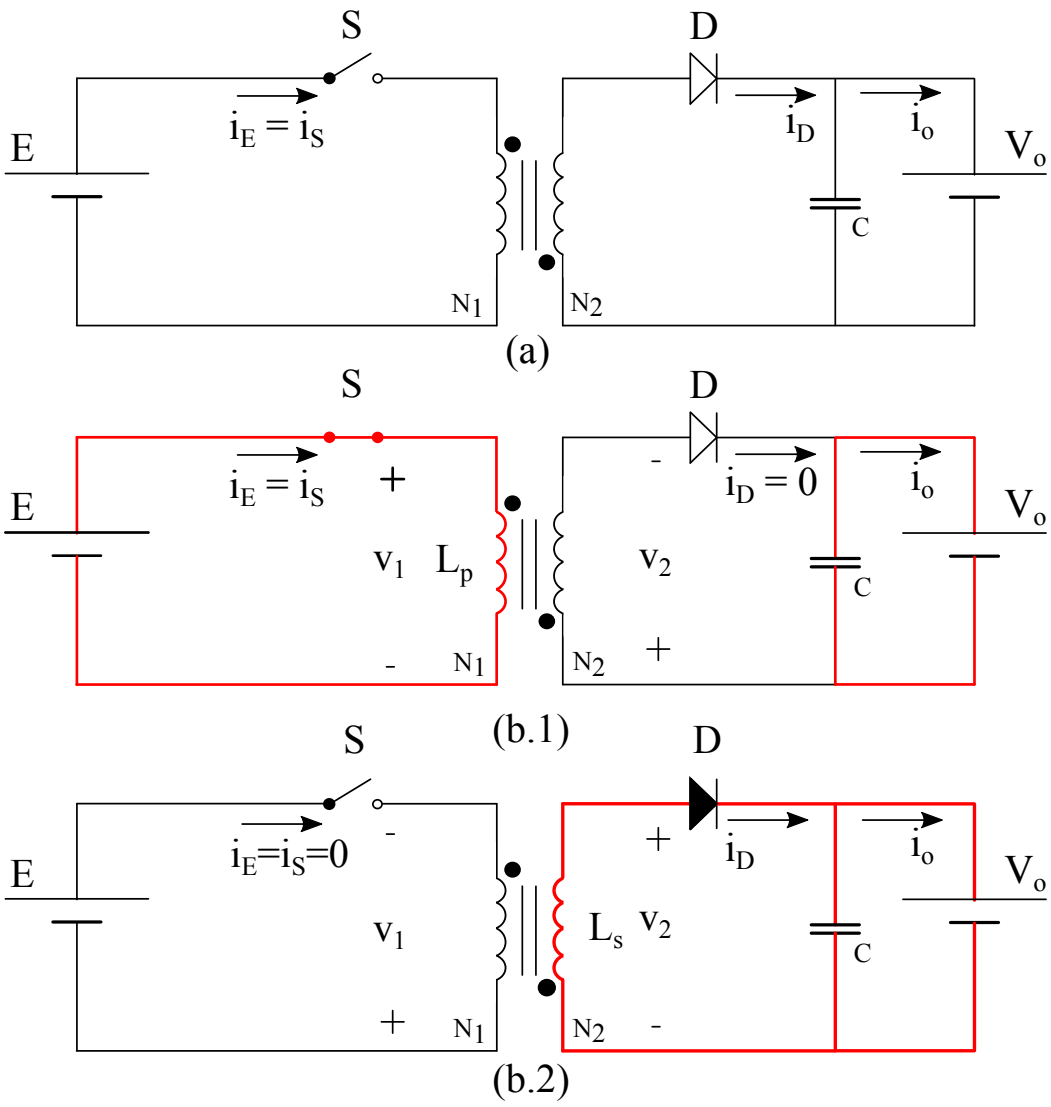

Figure 3.5: Flyback Converter.

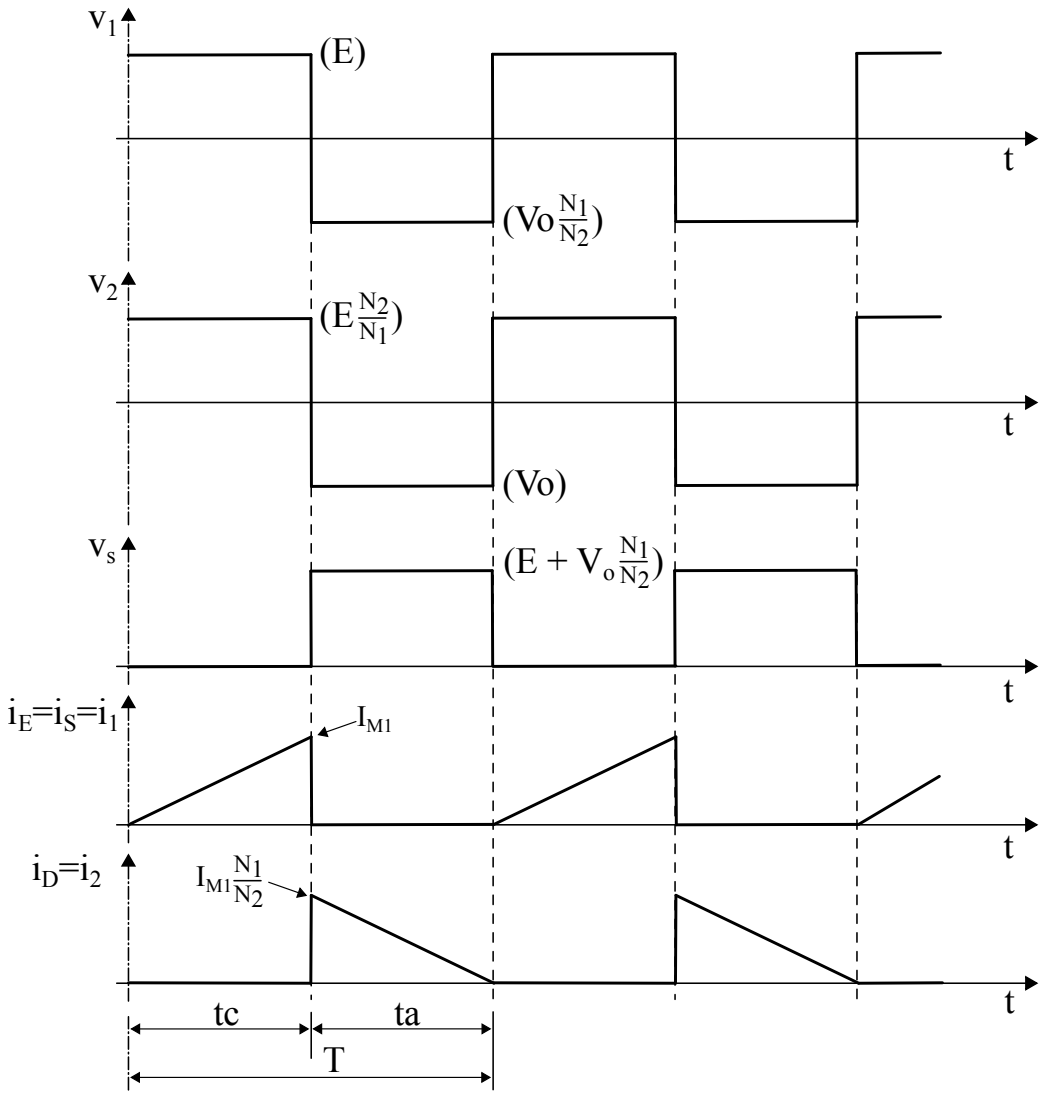

Figure 3.6: Flyback Converter Waveforms (DCM).

Chapter 4

Control Techniques, Analysis and Design

High level cell balancing can be achieved using either voltage based input or state-of-charge based input. Voltage based methods use simple hardware thus making their implementation easier, but suffer from slower balancing speeds and possibly introducing further imbalances due to distortions from impedance differences [43]. SoC based methods are much more complicated but are more accurate and faster to balance [43]. In this thesis, a top level controller balances the cells state-of-charge using actuating currents in the links. The state-of-charge x is not measurable but can be estimated according to $y = C(x)$ where y is the voltage associated with the battery terminals and C is some nonlinear mapping [24]. Kalman filters [25], neural networks [26], electrochemical impedance spectroscopy [27] and fuzzy logic [28, 29] are all examples of advanced methods for SoC estimation. This Chapter assumes SoC is constructed with sufficient precision. In this Chapter, different balancing control methods are identified and developed. These methods include a unconstrained optimization problem

using a Linear Quadratic Regulator (LQR) and finally a constrained optimization problem using Model Predictive Control (MPC). These methods are benchmarked against traditional rule based (RB) balancing.

4.1 Battery System Description

A description for the overall system must first be defined before developing the control algorithms. The redistributive non-dissipative balancing system known as the Multiple Transformer topology is shown Fig. 4.1. The battery pack is defined by n series connected battery cells with m number of links. Each cell is described by the amount of remaining charge via $\mathbf{Q}x \in \mathbb{R}^n$. The matrix

$$\mathbf{Q} = \begin{bmatrix} \widehat{C}_1 & 0 & \dots & 0 \\ 0 & \widehat{C}_2 & \dots & 0 \\ \vdots & \vdots & & \vdots \\ 0 & 0 & \dots & \widehat{C}_n \end{bmatrix} \in \mathbb{R}^{n \text{x} n}$$

is a diagonal matrix that defines each cells maximum charge capacities ($\widehat{C}$ in Ah) and x is the state-of-charge vector

$$x = \begin{bmatrix} x_1 & x_2 & \dots & x_n \end{bmatrix}^\top \in \mathbb{R}^n.$$

Each element in the SoC vector ranges between zero and one where the value of 0 corresponds to a completely empty cell and the value of 1 corresponds to a fully charged cell. For the system to become balanced, charge is moved between m links. The balancing current being transfered through the links is $\mathbf{A}u \in \mathbb{R}^m$ where u is a

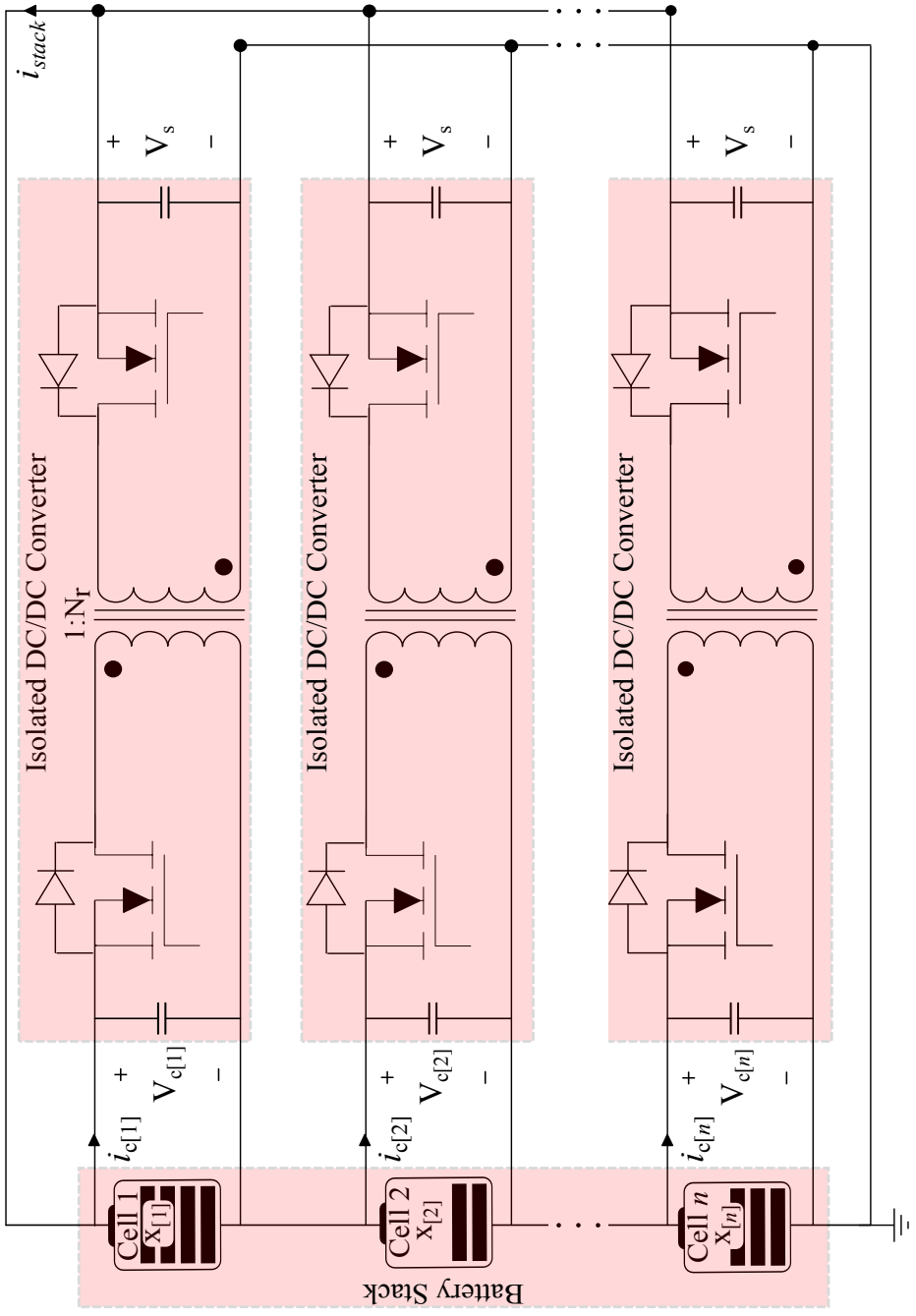

Figure 4.1: Multiple Transformer Balancing Topology (Flyback Converters).

vector containing the normalized balancing currents and

$$\mathbf{A} = \begin{bmatrix} \widehat{I}_1 & 0 & \dots & 0 \\ 0 & \widehat{I}_2 & \dots & 0 \\ \vdots & \vdots & & \vdots \\ 0 & 0 & \dots & \widehat{I}_m \end{bmatrix} \in \mathbb{R}^{m \times m}$$

defines a diagonal matrix containing the maximum current ($\widehat{I}$ in Amps) each link can handle.

The connection between n cells and m links is defined by a topology matrix $\mathbf{T} \in \mathbb{R}^{n x m}$. It describes how the balancing charge is transfered (from and to each cell). For the bi-directional multiple transformer topology shown in Fig. 4.1, $\mathbf{T}$ is defined in [5] as

$$\mathbf{T} = \begin{bmatrix} \frac{1}{n} - 1 & \frac{1}{n} & \dots & \frac{1}{n} \\ \frac{1}{n} & \frac{1}{n} - 1 & \dots & \frac{1}{n} \\ \vdots & \vdots & & \vdots \\ \frac{1}{n} & \frac{1}{n} & \dots & \frac{1}{n} - 1 \end{bmatrix} \in \mathbb{R}^{n \times m}.$$

For this topology, charge is removed from one cell and distributed equally amongst all the cells in the stack (C2S). Likewise, the charge can be removed from the entire stack then added to a single cell (S2C). Each cell has its own unique link to the stack that allows for simultaneous movement of charge to and from multiple cells. Thus, the charge stored in a battery cell is modeled using simple continuous time integrator

dynamics as

$$\mathbf{Q}\dot{x}(t) = \mathbf{TA}u(t), \tag{4.1}$$

where the topology matrix $\mathbf{T}$ relates the normalized balancing currents $u(t)$ with the SoC $x(t)$. A sign convention of $u(t) > 0$ indicates a flow of charge from the cell to the stack and $u(t) < 0$ indicates a flow of charge from the stack the cell. Since $\mathbf{T}$, $\mathbf{A}$, $\mathbf{Q}$ are all constants, the system dynamics can be simplified to

$$\dot{x}(t) = \mathbf{B}u(t), \tag{4.2}$$

where $\mathbf{B} = \mathbf{Q}^{-1}\mathbf{TA}_u$. With the addition of the topology matrix $\mathbf{T}$, equation 4.2 is identical to equation 1.1 but has been expanded for multiple cells. The maximum rated link current limits the applied balancing current. These balancing currents are subject to polyhedral constraints that depend on the topology [5] [44]. The inequality constraint is based on the maximum amount of current through each link $|u(t)| \leq 1$. From **Proposition 1** [5] there exists a constant input trajectory $u(t) = \bar{u}$. Thus, the state-of-charge is further simplified to just

$$x^+ = x + T_s\mathbf{B}\bar{u}, \tag{4.3}$$

where T_s is the sampling period and $\bar{u}$ is the normalized balancing currents found by each control method.

4.2 LQR Control

This method is first described in [37] but is expanded upon in this Thesis. The constraints for the system are written as $\mathbf{H}\bar{u} \leq K$ for the inequality constraint and $\mathbf{H}_{eq}\bar{u} = K_{eq}$ for the equality constraint. For the LQR control to function, the equality constraint on the system dynamics is defined by transforming (4.3) into a regulation problem using the transformation matrix

$$\mathbf{L} = \begin{bmatrix} 1 & -1 & 0 & \dots & 0 & 0 \\ 0 & 1 & -1 & \dots & 0 & 0 \\ \vdots & \vdots & \vdots & & \vdots & \vdots \\ 0 & 0 & 0 & \dots & 1 & -1 \end{bmatrix} \in \mathbb{R}^{(n-1)\times n}.$$

This matrix $\mathbf{L}$ leaves the difference in SoC between neighboring cells. Thus the regulation problem uses $\bar{x} = \mathbf{L}x$ and the balanced state is when $\bar{x} = 0$. The equality constraint is removed using the transformation

$$\bar{u} = \mathbf{F}u' + u_0, \tag{4.4}$$

where $\mathbf{F}$ is the nullspace of $\mathbf{H}_{eq}$, such that $\mathbf{F}\mathbf{H}_{eq} \equiv 0$ and u_0 is any solution of $\mathbf{H}_{eq}u_0 = \mathbf{K}_{eq}$. This will yield the system

$$\bar{x}^+ = \bar{x} + \bar{\mathbf{B}}u' + \mathbf{L}\mathbf{B}u_0, \tag{4.5}$$

where $\bar{\mathbf{B}} = \mathbf{L}\mathbf{B}\mathbf{F}$. The component $\mathbf{L}\mathbf{B}u_0$ is a non-zero offset value in general that can be removed by integration. However, $\mathbf{L}\mathbf{B}u_0 \equiv 0$ for all topologies studied in [5].

The updated system (4.5) is linear, thus a discrete, infinite-time Linear Quadratic Regulator (LQR) that minimizes the cost function $J = \sum_{k=0}^{\infty}(\bar{x}_k^T \mathbf{Q}\bar{x}_k + \bar{u}_k^T \mathbf{R}\bar{u}_k)$ is used.

The LQR problem is solved by a regular feedback controller defined as

$$u' = -\mathbf{K}_{lqr}\bar{x}, \tag{4.6}$$

where $\mathbf{K}_{lqr}$ is found by solving the discrete time Riccati equation. However, the controller input may not satisfy the inequality constraints. Thus, the input is saturated such that it satisfies the inequality constrains according to

$$\bar{\mathbf{H}}\bar{u} \leq \bar{K}, \tag{4.7}$$

where $\bar{\mathbf{H}} = \mathbf{HF}$ and $\bar{K} = K - \mathbf{H}u_0$. The result is transformed into a control input for the original system with (4.4). The saturation (4.7) ensures that the inequality constraints are satisfied and the transformation (4.4) ensures that the equality constraints are met. Meaning that the resulting back-transformed $\bar{u}$ is feasible. Also, the resulting closed loop system is stable according to [45] [46]. The LQR now has a control input $\bar{u}$ that defines the balancing currents in each link as

$$\mathbf{A}\bar{u} = [i_{c_1}, i_{c_2}, i_{c_3}...i_{c_m}]. \tag{4.8}$$

4.3 MPC Control

In [5] performance metrics have been developed to evaluate hardware. This thesis uses the minimum time to balance (t2b) metric as a balancing control. Defining this control is not as straight forward as LQR because it not only has to determine the normalized balancing currents, but must do so such that the balancing occurs in the minimum amount of time τ. Thus, a battery cells state of charge in terms of a control input at the final balancing time τ, is

$$x(\tau) = x(0) + \mathbf{B}\int_0^\tau u(t)dt. \tag{4.9}$$

From **Proposition 1** [5] there exists a constant input trajectory $u(t) = \bar{u}$ such that

$$x(\tau) = x(0) + \mathbf{B}\bar{u}\tau. \tag{4.10}$$

Much like the LQR method, the constraints for the system are written as $\mathbf{H}\bar{u} \leq K$ for the inequality constraint and $\mathbf{H}_{eq}\bar{u} = K_{eq}$ for the equality constraint. The equality constraint on the system dynamics is defined by transforming (4.10) into a regulation problem. However, with MPC the transformation matrix is

$$\mathbf{L} = \mathbf{I} - \mathbf{J} \tag{4.11}$$

where $\mathbf{I} \in \mathbb{R}^{nxn}$ is the identity matrix and $\mathbf{J} \in \mathbb{R}^{nxn}$ is a matrix containing all $1/n$ elements. This removes the average SoC and leaves the unbalanced SoC. The equality

constraint now becomes

$$\mathbf{L}x(0) + \mathbf{LB}\bar{u}\tau = \mathbf{L}x(\tau) = 0. \tag{4.12}$$

The constraints for the system are written as $\mathbf{H}\bar{u} \leq K$ for the inequality constraint and $\mathbf{H}_{eq}\bar{u} = K_{eq}$ for the equality constraint. The constrained linear optimization problem is formally expressed as

$$\tau^{\star}(x) = \underset{\tau \geq 0}{\text{minimize}}\, \tau \tag{4.13a}$$

$$\text{subject to } \mathbf{L}x + \mathbf{LB}\bar{u}\tau = 0 \tag{4.13b}$$

$$\mathbf{H}\bar{u}\tau - \mathbf{K}\tau \leq 0 \tag{4.13c}$$

To efficiently solve (4.13a) using popular Linear programming solver packages such as LPSOLVE, CPLEX or MOSEK, it is worth reproducing the problem in standard form. This is achieved by defining a new column vector containing both variables

$$z = \begin{bmatrix} v \\ \tau \end{bmatrix},$$

where $v = \bar{u}\tau$. It is important to realize that $\mathbf{L}x$ is a parameter and is treated as a constant. The minimum time to balance problem (4.13a) in standard form becomes

$$z^{\star} = \text{minimize}\, g'z \tag{4.14a}$$

$$\text{subject to } \mathbf{A}_{eq}z = b_{eq} \tag{4.14b}$$

$$\mathbf{A}z \leq b \tag{4.14c}$$

where $\mathbf{A}_{eq} = [LB\ 0]$, $b_{eq} = [-\mathbf{L}x\ 0]$, $\mathbf{A} = [\mathbf{H} - k], b = 0$.

Many simple solvers are more efficient when dealing without equality constraints such as qpOASES. This is not mandatory but by removing the equality constraint from (4.14a), the dimensions of the optimization problem are reduced.

To do this, the following linear transformation is used

$$z = \mathbf{F}\bar{z} + z_0 \tag{4.15}$$

where $\mathbf{F}$ is the nullspace of $\mathbf{A}_{eq},$ such that $\mathbf{F}\mathbf{A}_{eq} \equiv 0$ and z_0 is any solution of $\mathbf{A}_{eq}z_0 = b_{eq}$. Equation (4.15) is substituted into (4.14a) to ensure that the equality constraint is still satisfied but is now removed from the problem. Thus, a formal definition for the minimum time to balance problem in standard form with the removed equality constraint is

$$\bar{z}^{\star} = \text{minimize}\, g'\bar{z} \tag{4.16a}$$

$$\text{subject to } \bar{\mathbf{A}}\bar{z} \leq \bar{b} \tag{4.16b}$$

where $\bar{\mathbf{A}} = \mathbf{A}\mathbf{F}$, $\bar{b} = b - \mathbf{A}z_o$.

The performance metric is now used to define a model predictive controller. To adapt this into a discrete time MPC controller, equation (4.16a) is solved for the optimal τ^* and $\bar{u}^*$ at each sampling time instant kT_s using the discrete time dynamics

$$\mathbf{L}x + \mathbf{L}\mathbf{B}\bar{u}\tau = 0. \tag{4.17}$$

Then a scaling factor ν is introduced to scale down the control if τ^* is smaller than the

sampling period T_s such that the process leads to the following closed loop dynamics

$$x[k+1] = x[k] + \nu T_s \mathbf{B} \bar{u}^*[k] \tag{4.18}$$

where

$$\nu = \begin{cases} \frac{\tau^*}{T_s} & \text{for } \tau^* \leq T_s \\ 1 & \text{for } \tau^* > T_s \end{cases} \tag{4.19}$$

This sequence is repeated for each sampling instant until the system becomes balanced, i.e $\mathbf{L}x[k] = 0$.

4.4 Rule based Control

Rule based control methods use a set of rules to manipulate some form of outcome in a system. Examples of RB in other EV applications are found in [47–49]. For a bi-directioanl (C2S/S2C) system, the average state-of-charge is defined as

$$\bar{x} = \frac{||x||_1}{n} \tag{4.20}$$

where x is a vector containing state-of-charge and n is number of cells. If a cells x is higher than the average $\bar{x}$ then it is discharged onto the stack i.e $\bar{u} = 1$. Likewise, if a cells x is lower than the average $\bar{x}$ then it is charged by the stack i.e $\bar{u} = -1$. As a side note, this could easily be changed for a uni-directional active dissipative approach by balancing towards the minimum SoC. This simple control method uses the maximum link current available i.e each cell is always charging or discharging until all cells SoC

fall within a "balanced region" B_z. A transformation matrix is used

$$\mathbf{L} = \mathbf{I} - \mathbf{J} \tag{4.21}$$

where $\mathbf{I} \in \mathbb{R}^{nxn}$ is the identity matrix and $\mathbf{J} \in \mathbb{R}^{nxn}$ is a matrix containing all $1/n$ elements. This removes the average SoC and leaves the unbalanced SoC. Thus the balanced region B_z is defined as 5% or when

$$||\mathbf{L}x||_1 < 0.05 \tag{4.22}$$

The set of simple rules for redistributive non-dissipative balancing are summarized as

$$\bar{u} = \begin{cases} 1(Discharge) & \text{if } x > \bar{x} \\ -1(Charge) & \text{if } x < \bar{x} \\ 0 & \text{if } ||\mathbf{L}x||_1 < 0.05 \end{cases} \tag{4.23}$$

Chapter 5

Implementation Details

5.1 Linear Technology DC2100A Hardware

At the outset of this thesis, implementing control strategies and obtaining experimental data as such was most important. For rapid prototyping and implementation, the hardware for experimental data was built upon an existing Linear Technology DC2100A Demonstration board [50]. This application hardware is developed for bi-directional cell balancing of up to 12 Lithium ion cells. By monitoring the cell voltage and protecting against over charge and under charge conditions, algorithms for State-of-charge estimation can be embedded onto a daughter board (PIC18F47J53). This microcontroller communicates to the LTC3300-1 and LTC6804 integrated circuits through SPI communication.

Off the shelf this board had bi-directional flyback converters that were all controlled with a convenient graphical user interface. The original Code Communication Diagram in Fig. 5.1 shows the flow of communication such that any new software communicates with the boot firmware through the HID windows driver. The GUI

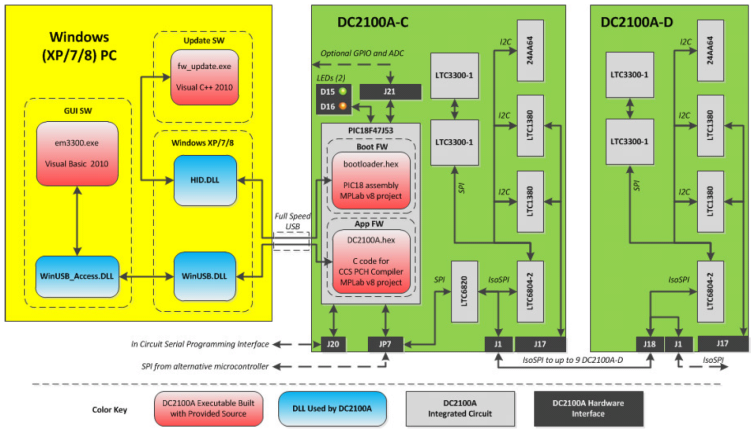

Figure 5.1: DC2100A Code Communication Diagram [7].

software communicates with the Application Firmware through the WinUSB windows driver. The App FW passes commands and responds to the GUI SW. The App FW must also provide communication to the ICs and general inputs and outputs. The main ICs on the DC2100A are the LTC6820, LTC6804-2 and LTC3300-1. The LTC6820 IC converts SPI into isoSPI for the monitoring ICs on the DC2100A. The LTC6804-2 IC measures battery voltage as well as passes I^2C and SPI communication to the balancing chips. The LTC3300-1 IC provides active balancing commands to the bi-directional converters.

On the surface this board seemed to have what was required for conducting the experiments with little to no modifications. However, during the initial stages of testing, it became clear that the on-board PIC microcontroller did not have sufficient storage space for any additional algorithms. Luckily, the designers at Linear Technology made it possible to disconnect the PIC from the system then connect an alternative solution to monitor and control the DC2100A hardware. This is done through the JP7 header seen in the original communication diagram (Fig. 5.1). The JP7 header is a 6 row pin configuration that interfaces with alternative microcontrollers via SPI

and has a pinout as follows: pin 1 - LTC6820 ENABLE, pin 2 - SPI MOSI, pin 3 - SPI MISO, pin 4 - SPI SCK, pin 5 - SPI CS, pin 6 - GND.

5.2 Texas Instruments F28377D Controller

The alternative microcontroller that was selected for this thesis was a Texas Instruments (TI) TMS320F28377D microcontroller. The reason this was the chosen one was because it boasts dual core architecture with two 32-bit CPUs operating at 200 Mhz. It also had a lot more storage than the original PIC controller with 1 MB of Flash and 204 KB of RAM. However, all new software was required to proceed for the F28377D to function as the main balancing controller. All communication was done via SPI, therefore integrating this software was paramount to the success of operating the balancing controller. Fig. 5.2 Shows the waveforms measured by the oscilloscope for SPI communication.

Other important functions that were ported over from the PIC to the main balancing controller (F28377D) were monitoring voltage cells via a *read_voltages* command, clearing any data stored on the registers such that clean messaged could be sent as well obtaining over voltage and under voltage flags that were important for safety. Furthermore, the added algorithms for balancing control were added onto the second core of the DSP. Other important software modifications was in a state-of-charge estimation lookup table based on the cells OCV.

Figure 5.2: Oscilloscope SPI protocol with TMS320F28377D and DC2100A.

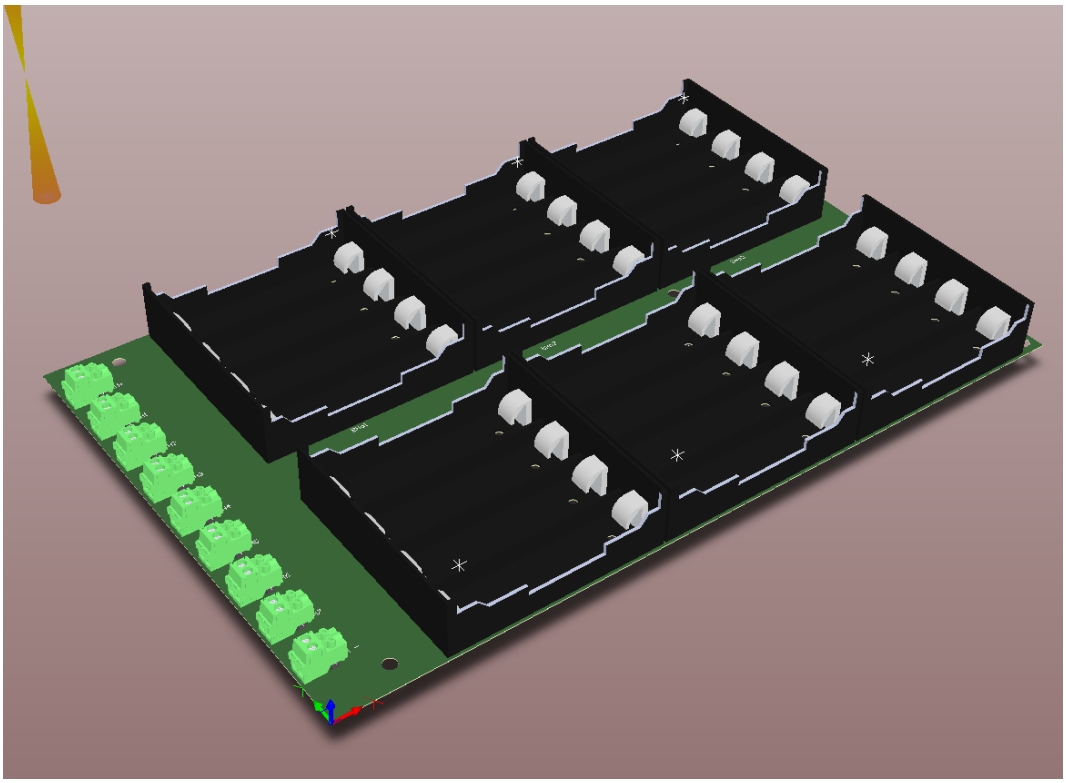

Figure 5.3: Battery Balancing 3D Graphic of Harness.

5.3 Pack Harness

A battery pack test harness was first designed in Altium then assembled in house. It was specifically designed for Lithium-ion 18650 type cells with known dimensions. This pack harness is capable to housing up to 6 modules in series, each module can contain up to 4 cells in parallel. The layout of the harness was chosen based on ease of access to each cell. It is strictly used for demonstration purposes and pack verification. A 3D simulated model is shown in Fig. 5.3 and the PCB trace layout in Fig. 5.4.

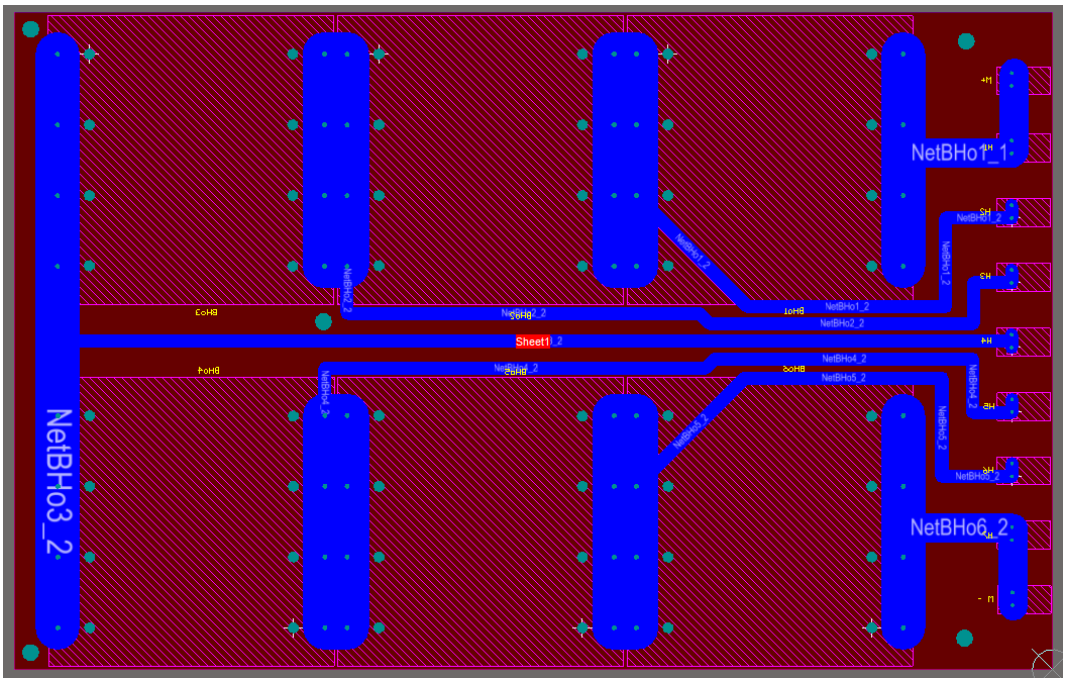

Figure 5.4: Battery test harness Altium PCB trace layout.

5.4 Full Test Bench

To showcase the redistributive non-dissipative balancing approach, experiments are conducted on the test bench shown in Fig. 5.5. To summarize the full test bench, the first component in the system is a modified DC2100A demo board from Linear Technology. On this board is a LTC-6804 monitoring chip that measures the cells voltages. It has internal over/under voltage protection and conveys the information via SPI to the control DSP. It also features a LTC-3300 chip that controls the MOSFET for the Flybacks converters. Each flyback module operates in critical mode utilizing a pulse frequency modulation (PFM) strategy descried in [37]. How this works is when the primary switch for a module is closed while discharging a cell, it measures the instantaneous primary current until a maximum peak current is reached. It then opens the

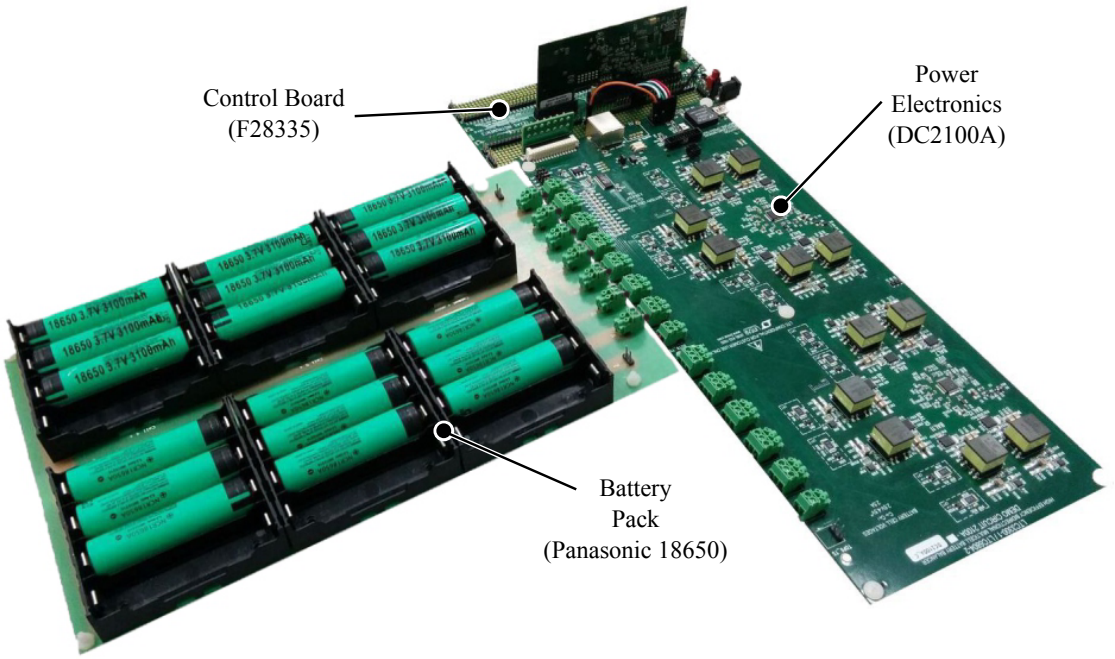

Figure 5.5: Test bench.

primary switch and closes the secondary switch to allow the instantaneous secondary current to be released back onto the stack. From the LTC 3300 data sheet available online [8], the waveforms are shown in Fig. 5.6.

The second component is a custom built test harness which houses the battery pack using Panasonic NCR 18650 cells. The battery pack consists of 6 modules connected in series. Each module has 2 Lithium Ion battery cells connected in parallel. The last component in the system is a Texas Instruments F28377D dual core microcontroller (DSP). The primary function of core one is to solve for the optimal normalized balancing current based on the cells state-of-charge for the MPC control method. The solver was written in Matlab as functions blocks, then code compiled into C files using Matlab Coder. This way of working allows for fast prototyping and comparison between a simulated and experimental environment. The second core

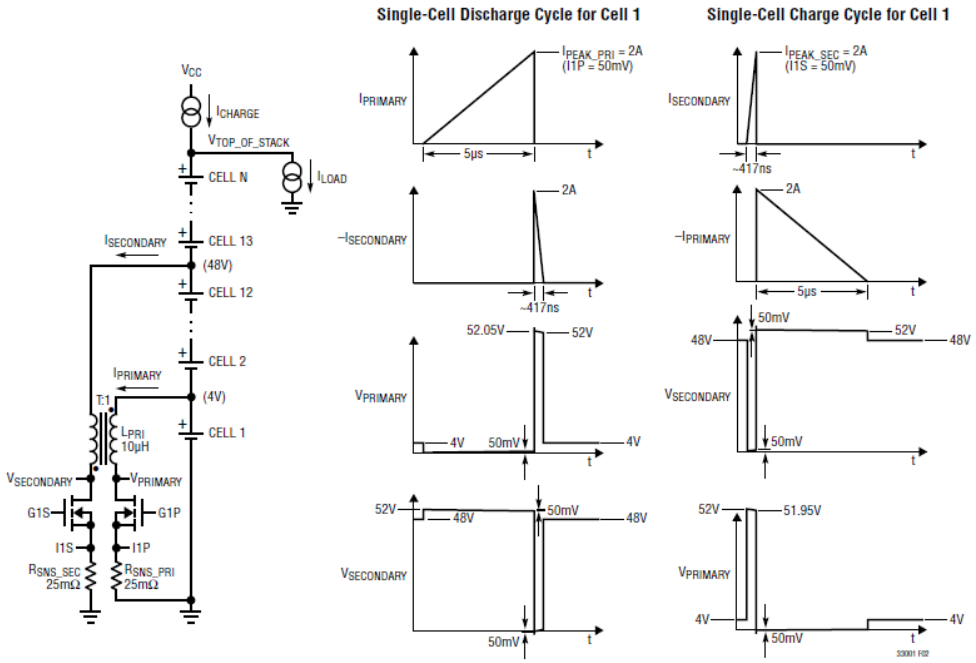

Figure 2. Synchronous Flyback Balancing Example with T = 1, S = 12

Figure 5.6: LTC DC2100A simplified schematic and operational waveforms [8].

handles all Battery Management type activities and is connected through SPI to the DC2100A demo board. Its main tasks are to read cell voltage, determine SoC, control the on time for each MOSFET, and to send information to core 1.

5.5 Low Level Control

To actuate the desired current from control method i.e RB, LQR and MPC, a upper level, low frequency control strategy referred to as constant operating point modulation (COPM) must be utilized [37]. The actuation can be applied by keeping a constant operating point in low level control. The implemented Flyback converter is either *on* transferring a given current or *off*. This type of operation is suitable

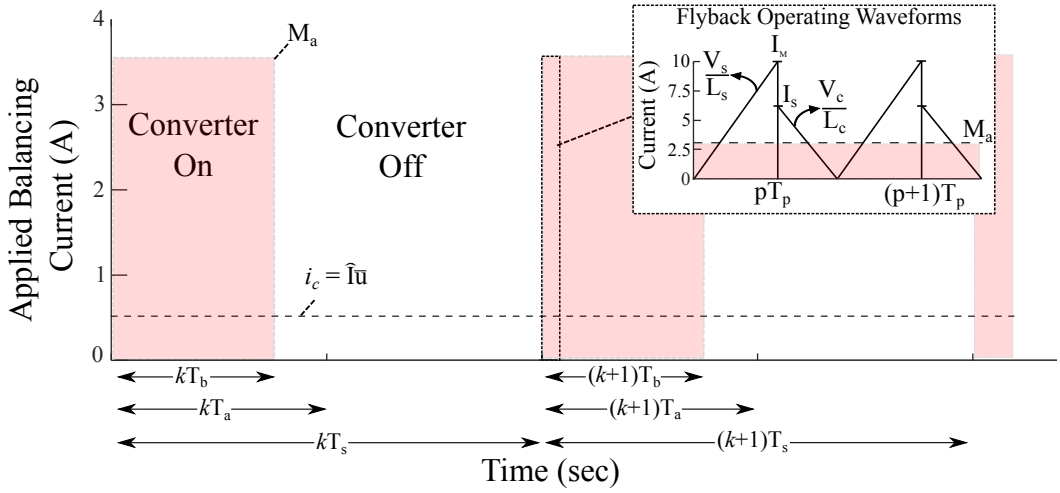

Figure 5.7: Low Level Control Switching Waveforms.

for battery balancing but requires a high level PWM. The actuator applies an average current by keeping the DC/DC converter on for a certain amount of time and turns it off for the rest. COPM is implemented strictly due to how the LTC-3300 IC from Linear Technology performs its low level control. This strategy can be better understood by looking at Fig. 5.7.

The high level controller (RB, LQR, MPC) uses a smaller current due to this on/off type of low level control. In reality, the hardware is operating with a higher current of M_a but only for a maximum time of T_a. The relationship between what the high level control thinks the batteries are operating with ($i_c = \widehat{I}\bar{u}$) and what is actually being delivered to the batteries (M_a) is

$$\widehat{I}_L = \frac{M_a T_a}{T_s}. \tag{5.1}$$

At each kT_s time step, i_c is translated into an effective current that works with the COPM strategy. This is shown in Fig. 5.7. Since the LTC-DC2100A did not come

equipped with average link current sensors, estimated current equations provide a close approximation of the average link current through each flyback converter [37]. While a cell is being discharged, the estimated current through the link is

$$\widetilde{i}_d = \frac{I_M V_s}{2(V_s + N_r V_c)}. \tag{5.2}$$

While a cell is being charged, the estimated current through the link is

$$\widetilde{i}_c = \frac{I_S N_r V_s}{2(V_s + N_r V_c)}. \tag{5.3}$$

The values of the estimated currents are then scaled with the maximum operating link current M_a. These calculations are performed by the DSP in order to control how long each switch is on for T_b to achieve the same effective current the fast MPC controller requires. This on-time is calculated as

$$T_b = \begin{cases} \dfrac{\bar{u} M_a T_a}{\widetilde{i}_d} & \text{for } \bar{u} > 0 \\ \dfrac{-\bar{u} M_a T_a}{\widetilde{i}_c} & \text{for } \bar{u} < 0 \\ 0 & \text{for } \bar{u} = 0 \end{cases} \tag{5.4}$$

As a proof of concept test in [37] for the estimation equations 5.2 and 5.3, a constant discharge test was conducted on the first cell in the stack as shown by Fig. 5.8. At the beginning of discharge, the measured current is 3.697A which was obtained using a ammeter in the direct path of the first link. The estimated current for that link was 3.685A. At the end of discharge, the measured current is 3.851A. The estimated current for that link was 3.853A.

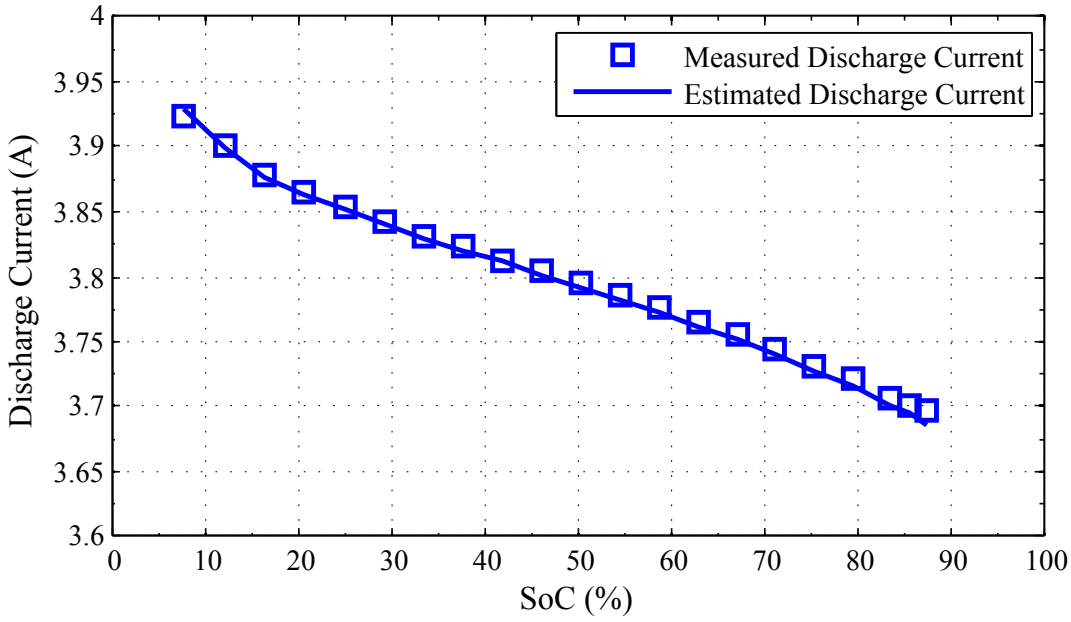

Figure 5.8: Measured vs. Estimated Link Currents.

5.6 Test Procedure and Graphical User Interface

For many microcontrollers available from Texas Instruments, a Simulink Coder (Formerly Real-Time Workshop) can be used to generate and execute C and C++ code from Simulink diagrams and Matlab functions automatically. However, at the time of writing this thesis, the TI DSP (F28377D) was not a working target for this method of programming. Thus, skills were developed in Code Composer Studio (CCS) by reading forums, data sheets and developing workshops. For the integration between the F28377D and DC2100A, low level software was programmed directly in CCS such as SPI communication, PWM signals and ADC inputs. However, for the more complicated high level RB, LQR and MPC balancing algorithms, scripts were developed in Matlab then flashed onto the DSP using embedded MATLAB (Matlab Coder) to generate C-code. This process is shown in Fig. 5.9 and is fundamentally different and

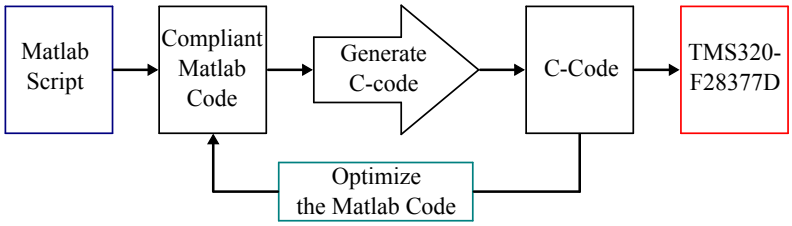

Figure 5.9: Programming with Matlab Coder for DSP.

more challenging than using Simulink Coder. The Matlab scripts had to essentially be open functions for parsing or solving data. A timer and clock was used for a rudimentary scheduler of tasks such as monitoring voltage, estimating SoC, turning balancing on and off as well as halting if any flags were triggered.

For each control method, the 6 series connected battery cells are charged independently using a Lithium-Ion charger until they reached an arbitrary deviation in voltage. The cells are then rested for 2 hours and a open circuit voltage is measured for the start of balancing sequence. This process was repeated until the cells starting SoCs and OCVs were close to one another for each test. To fully encapsulate the balancing efficiency, the system was turned off after balancing and rested for 1 day. The open circuit voltages and State-of-charge values were then recorded representing a final balanced system. A graphical user interface was coded and designed in Code composer studio GUI. This was written in Java to send and receive commands to the DSP in real time. It also recorded any error flags, cells measured voltages, estimated state-of-charge as well as estimated link currents and is shown in Fig. 5.10.

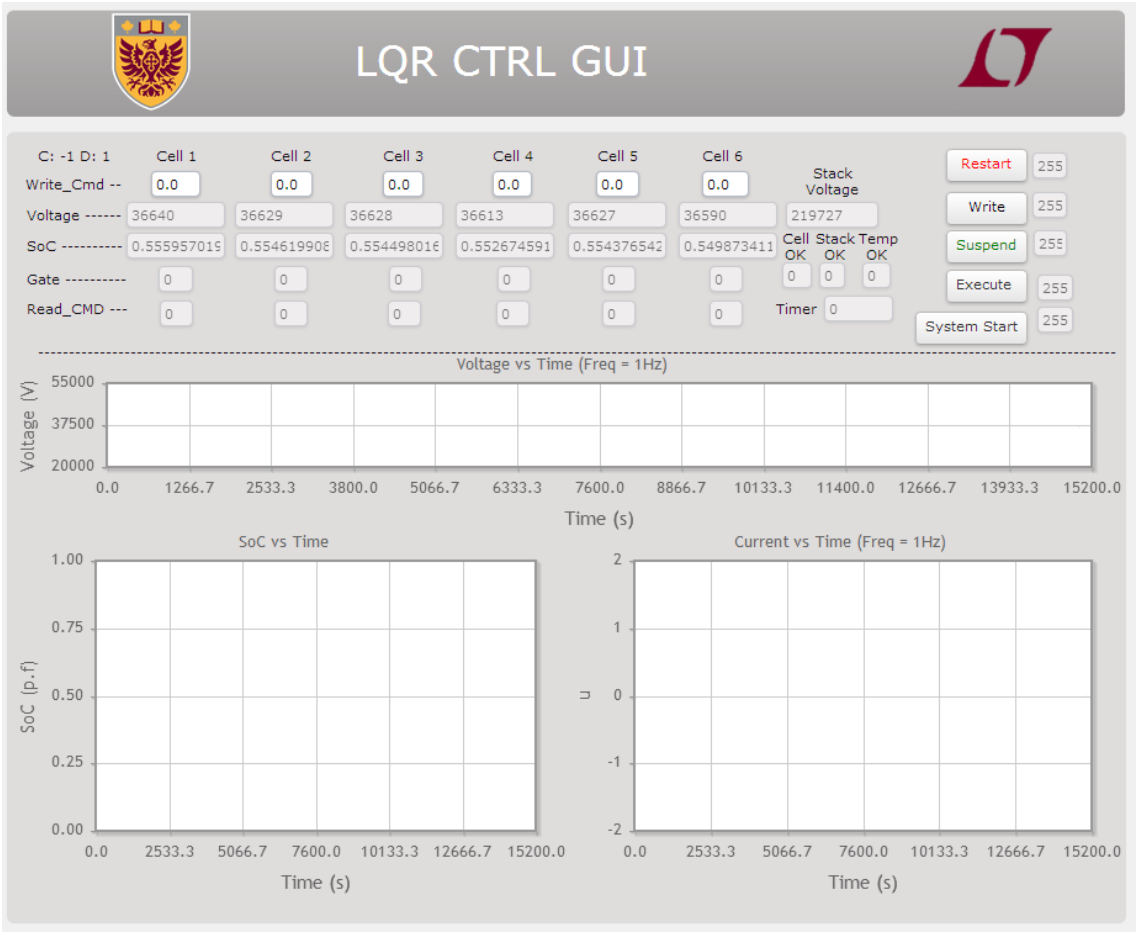

Figure 5.10: Graphical User Interface for Battery Balancing.

Chapter 6

Simulation results and Experimental validation

For this thesis, different battery balancing control methods have been simulated using MATLAB. The simulation scripts for each control method can be found in the Appendix of this Thesis. The closed loop system is compared with that of an experimental one. An evaluation of the controller and balancing hardware for a system containing 6 cells in series, each with a rated capacity of $\widehat{C} = 6.14Ah$ and each link with a maximum of $\widehat{I} = 0.875A$. The balancing hardware is carried out using flyback converters between each cell connecting to the stack of batteries in a individual cell to stack topology. The control methods being compared (defined earlier) are Rule based control (RB), Linear Quadratic Regulator Control (LQR) and Model Predictive Control (MPC). Each method has advantages and disadvantages alike and have an associated time to balance. The linear battery model used in simulation is represented

as

$$x[k+1] = x[k] + T_s \mathbf{B} \bar{u}, \tag{6.1}$$

where k is the discrete time step, $\mathbf{B}$ relates max link current with battery capacity and $\bar{u}$ are the normalized balancing currents defined by each control method. A sign convention of $\bar{u} > 0$ indicates a flow of charge from the cell to the stack (discharge) and $\bar{u} < 0$ indicates a flow of charge from the stack the cell (charge).

Similarly, experimental results are obtained using the experimental test bench in Fig. 5.5. This test bench is comprised of a LTC DC2100A Demo board equipped with bi-directional flyback converters and a custom built battery pack using Panasonic NCR 18650 cells. Six modules are placed in series making the pack (two cells per module). SoC is assumed to be reconstructed with sufficient precision but in reality a OCV Vs. SoC Lookup table is used. According to [51], a specification of balanced is defined when all battery cells state-of-charge are within a 3% margin. This margin will also be adapted for this research but it must be noted that SoC is more difficult to estimate with a high precision, which is not the focus of this thesis. At the end of balancing, a 1 day rest period is given to allow relaxation of the cells and more accurate balancing deviation can be captured and verified against the 3% margin.

Moreover, a new performance metric is introduced for battery balancing. The balancing hardware and control strategies have a associated balancing efficiency (η_B). This efficiency is attributed to the amount of unbalanced energy and the lost energy while balancing. If the DC-DC converters operated with 100% efficiency and there were zero losses due to the battery and connections, then the balancing efficiency would equal to one.

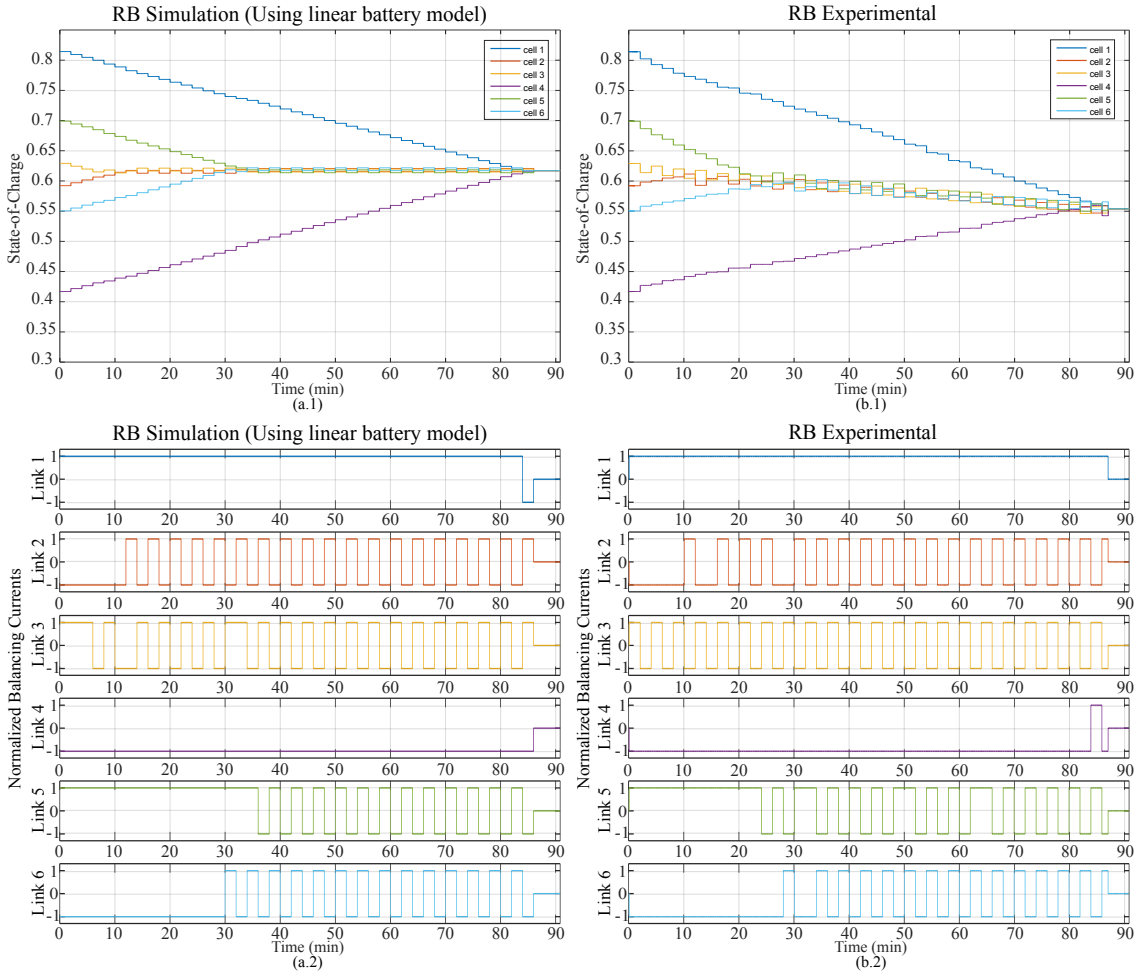

Figure 6.1: RB Simulation and Experimental Results.

6.1 Rule Based Control Strategy

Rule based control methods compare the average SoC to each cells SoC in the stack. During the balancing time, the current flowing through each cell is always the maximum. Balancing is stopped when all cells reach a predefined balancing zone. The RB controller described in Chapter 4 is simulated in MATLAB, then implemented on the experimental test bench. This high level balancing controller balances the state-of-charge using the normalized balancing currents shown in Fig. 6.1.

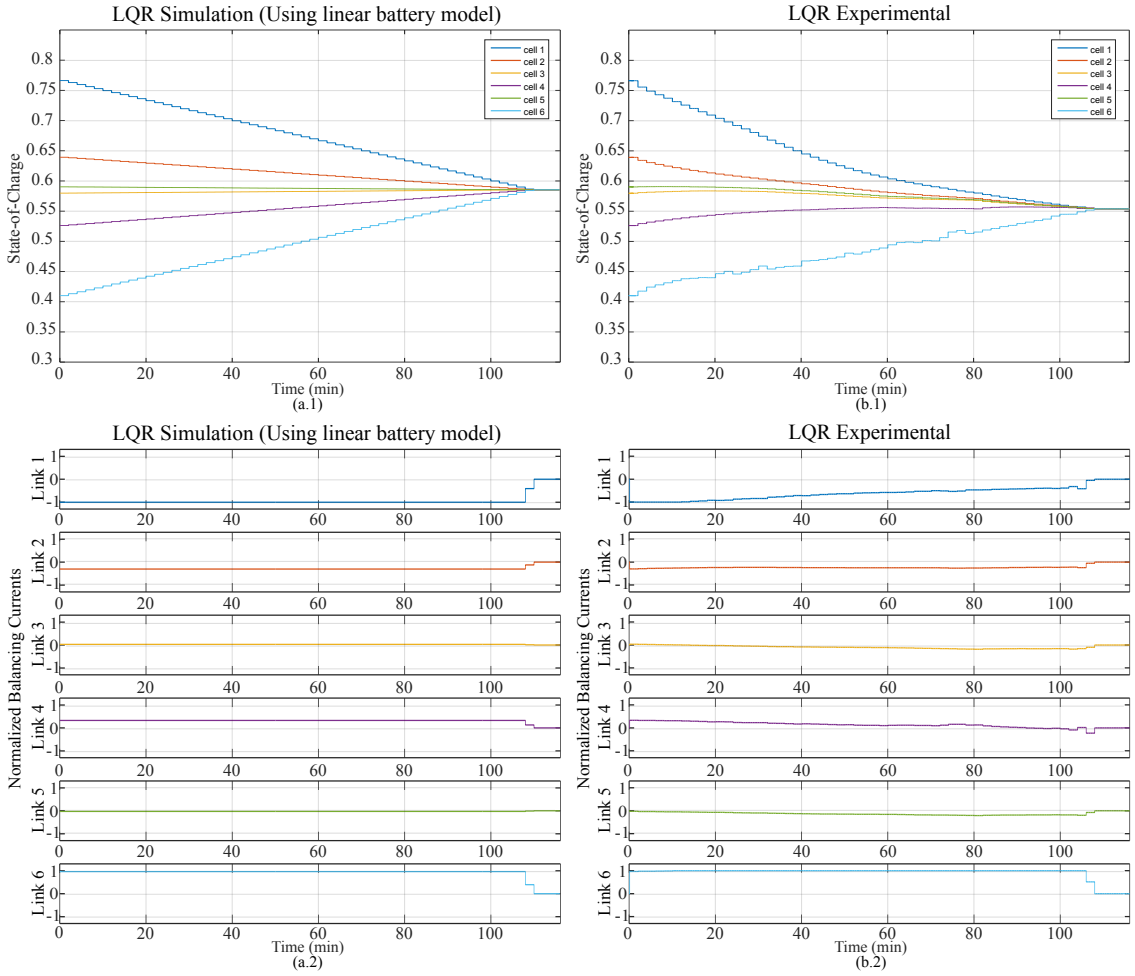

Figure 6.2: LQR Simulation and Experimental Results.

6.2 Linear Quadratic Regulator Control Strategy

The LQR control method uses Linear transformations to rewrite the balancing problem as a regulation problem that can be solved by saturating the solution. The LQR controller described in Chapter 4 is simulated in MATLAB, then implemented on the experimental test bench. This high level balancing controller balances the state-of-charge using the normalized balancing currents shown in Fig. 6.2.

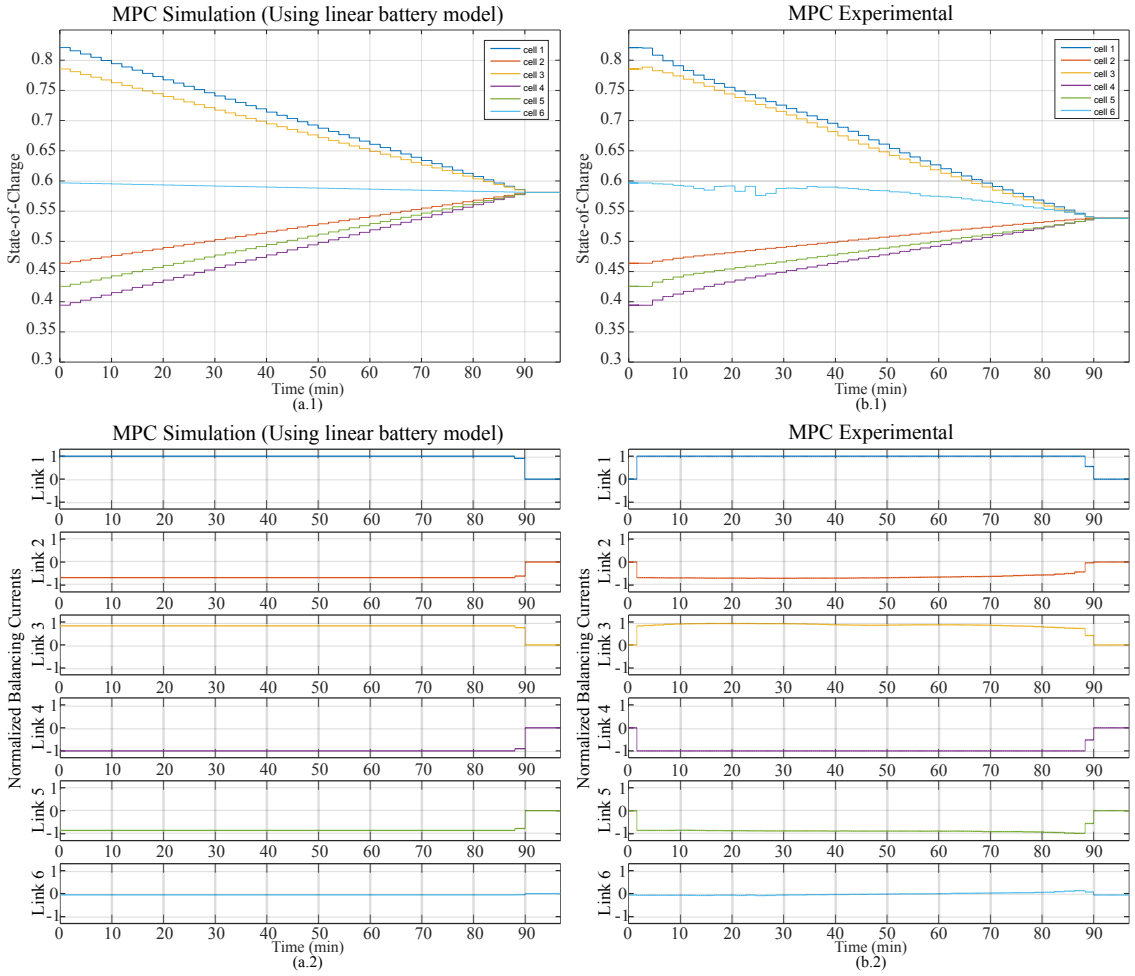

Figure 6.3: MPC Simulation and Experimental Results.

6.3 Model Predictive Control Strategy

The MPC optimization problem uses performance metrics from [5] to balance the SoC in the battery pack using constant current trajectories in minimum time. The MPC controller described in Chapter 4 is simulated in MATLAB, then implemented on the experimental test bench. This high level balancing controller balances the state-of-charge using the normalized balancing currents shown in Fig. 6.3.

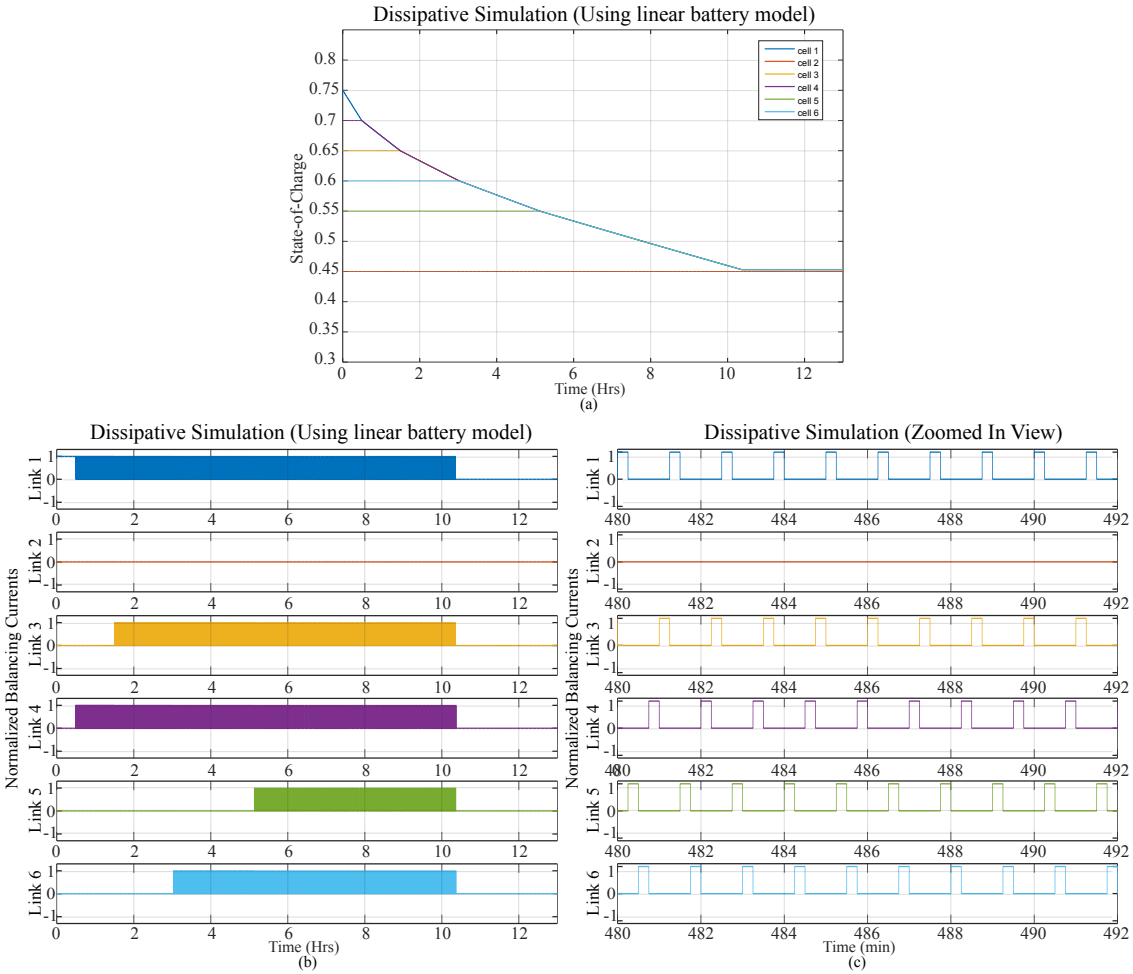

Figure 6.4: Dissipative Simulation and Experimental Results.

6.4 Dissipative Topology for comparison

A dissipative topology is shown for comparison. It utilizes a modified RB control method that dissipates excess energy from strong cells. The current flowing through each cell is dictated by the parallel resistance value. This topology is simulated in MATLAB. This high level balancing controller balances the state-of-charge using the normalized balancing currents shown in Fig. 6.4.

6.5 Balancing Efficiency

For a battery pack with n series connected cells with m number of links, the amount of initial charge stored in the battery cells is $\mathbf{Q}x_0 \in \mathbb{R}^n$. The diagonal matrix

$$\mathbf{Q} = \begin{bmatrix} \widehat{C}_1 & 0 & \dots & 0 \\ 0 & \widehat{C}_2 & \dots & 0 \\ \vdots & \vdots & & \vdots \\ 0 & 0 & \dots & \widehat{C}_n \end{bmatrix} \in \mathbb{R}^{nxn}$$

defines each cells maximum charge capacities ($\widehat{C}$ in Ah), and the initial state of charge vector x_0 is the amount of initial stored charge normalized by the total charge capacity. Each element in the x_0 vector ranges between zero and one where the value of 0 corresponds to a completely empty cell and the value of 1 corresponds to a fully charged cell. Furthermore, the matrix

$$\mathbf{V}_0 \in \mathbb{R}^{nxn},$$

defines another diagonal matrix containing the initial measured voltages (V) for each cell.

A balanced point about the initial average SoC is the column vector

$$\bar{x}_0 = \mathbf{J}x_0 \in \mathbb{R}^n,$$

where $\mathbf{J} \in \mathbb{R}^{nxn}$ is a matrix containing all $1/n$ elements. The difference in SoC each

cell is from this average is $\dot{x} = x_0 - \bar{x}_0$. Thus, the total initial unbalanced energy is

$$E_U = ||\mathbf{M}\dot{x}||_1$$

where $\mathbf{M} = \mathbf{V}_0\mathbf{Q}$. Similarly, the final SoC vector is defined as $x(\tau)$ where τ represents the time at which the system is balanced. Again, a diagonal matrix $\mathbf{V}_\tau \in \mathbb{R}^{nxn}$ defines the final measured voltages (V) for each cell. The difference in SoC each cell is from the initial average, $\dot{x}_\tau = x(\tau) - \bar{x}_0$, dictates how much total energy has been lost in the system. Thus, the total energy lost is

$$E_L = ||\mathbf{M}_\tau \dot{x}_\tau||_1$$

where $\mathbf{M}_\tau = \mathbf{V}_\tau\mathbf{Q}$.

A balancing efficiency performance metric is the overall effectiveness to redistributive the energy between the series connected cells while balancing. This metric can be used by any balancing hardware and control implementation. It is used in this thesis to compare the experimental results obtained in Fig. 6.1, Fig. 6.2 and Fig. 6.3. It can be described in words as the total amount of final additional energy E_A divided by the total amount of initial unbalanced energy E_U. It is now formally defined as

$$\eta_B = \frac{E_A}{E_U} = \frac{E_U - E_L}{E_U}$$

where E_L is the energy lost due to balancing. Most of this loss can be attributed to the power electronic energy conversion efficiency [15, 52, 53] and the battery cells coulombic efficiency [10, 54], . The balancing efficiency ranges between zero and one

where the value of 0 corresponds to all the unbalanced energy being lost i.e dissipative balancing and the value of 1 corresponds to perfect balancing with no losses in the system.

6.6 Discussion

According to [51], a specification of balanced is defined when all battery cells SoC is within a 3% margin. This thesis will try to define a more aggressive margin set of 2% difference between all SoC values. It must be noted that with a more accurate SoC estimation strategy and low level control strategy, this value margin will decrease substantially.

The RB experimental test started with an initial set of start-of-charge values in 6 cells as

$$x_0 = [0.82,\ 0.59,\ 0.63,\ 0.42,\ 0.70,\ 0.55]$$

for cells 1 through 6 respectively The initial voltage set (volts) for the same corresponding cells were

$$V_0 = \text{diag}[3.9023,\ 3.695,\ 3.7294,\ 3.5712,\ 3.7968,\ 3.6595]$$

The test originally started with an arbitrary unbalance of 40% difference in maximum and minimum SoC and 331mV in starting voltages. At the end of balancing and after the predefined rest period, this system had a ending set of start-of-charge values equivalent to

$$x_\tau = [0.56,\ 0.55,\ 0.56,\ 0.54,\ 0.56,\ 0.55]$$

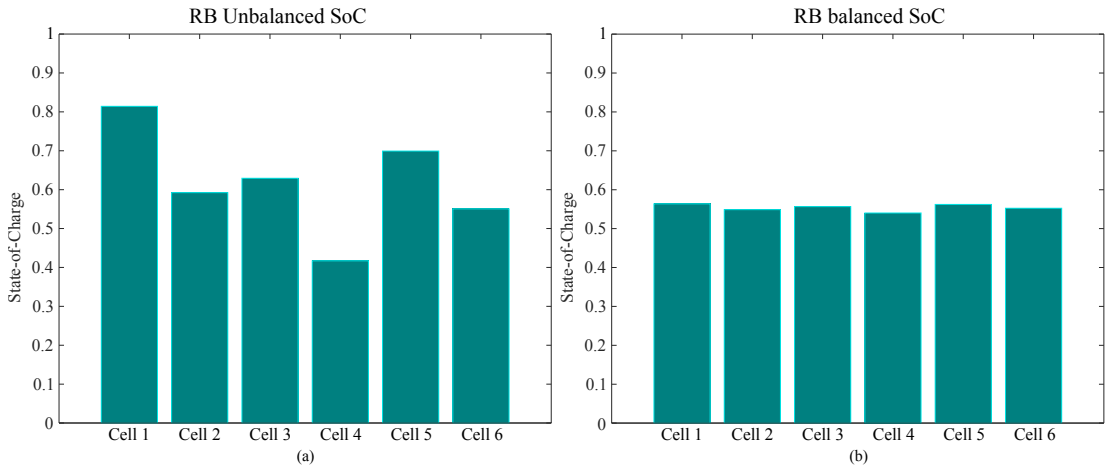

Figure 6.5: RB Unbalanced(a); Balanced(b) State-of-Charge.

The final voltage set in volts was

$$V_0 = \text{diag}[3.6703,\ 3.6581,\ 3.6645,\ 3.6514,\ 3.6691,\ 3.6610]$$

This shows the test ended with just a 2% difference in maximum and minimum SoC was achieved with 18.9mV difference in final voltages. According to the balance margin, RB was able to successfully balance the cells state-of-charge. However, the balancing efficiency for the RB method was calculated to be 0.36, due to the lost energy of the intermediate cells being charge and discharged until the end.

For the LQR experimental test, an initial set of start-of-charge values was

$$x_0 = [0.77,\ 0.64,\ 0.58,\ 0.52,\ 0.60,\ 0.41]$$

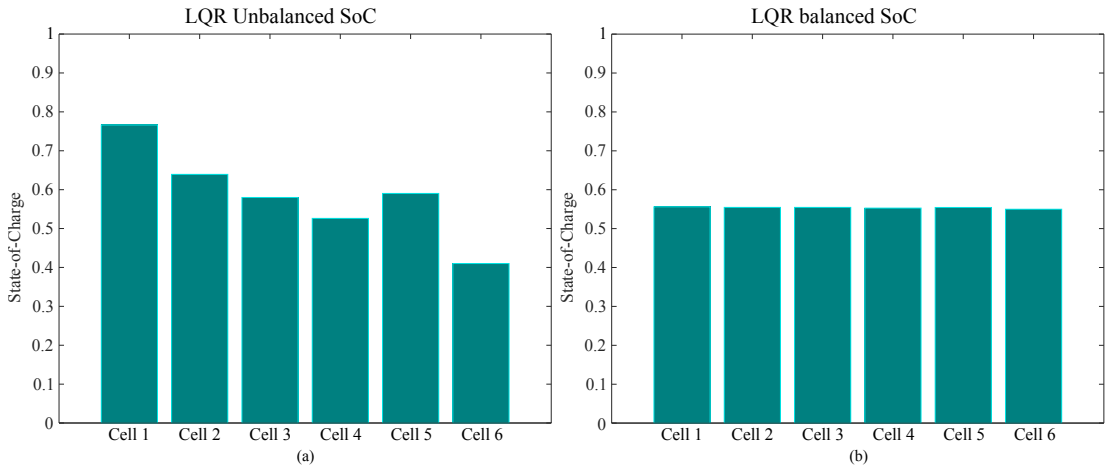

Figure 6.6: LQR Unbalanced(a); Balanced(b) State-of-Charge.

for cells 1 through 6 respectively. The initial voltage set (volts) for the same corresponding cells was

$$V_0 = \text{diag}[3.8582,\ 3.7393,\ 3.6841,\ 3.6409,\ 3.6933,\ 3.567]$$

The test originally started with an arbitrary unbalance of 36% difference in maximum and minimum SoC and 291mV in starting voltages. At the end of balancing and after the predefined rest period, this system had a ending set of start-of-charge values equivalent to

$$x_\tau = [0.56,\ 0.55,\ 0.55,\ 0.55,\ 0.55,\ 0.55]$$

The final voltage set in volts was

$$V_0 = \text{diag}[3.6640,\ 3.6629,\ 3.6628,\ 3.6613,\ 3.6628,\ 3.6590]$$

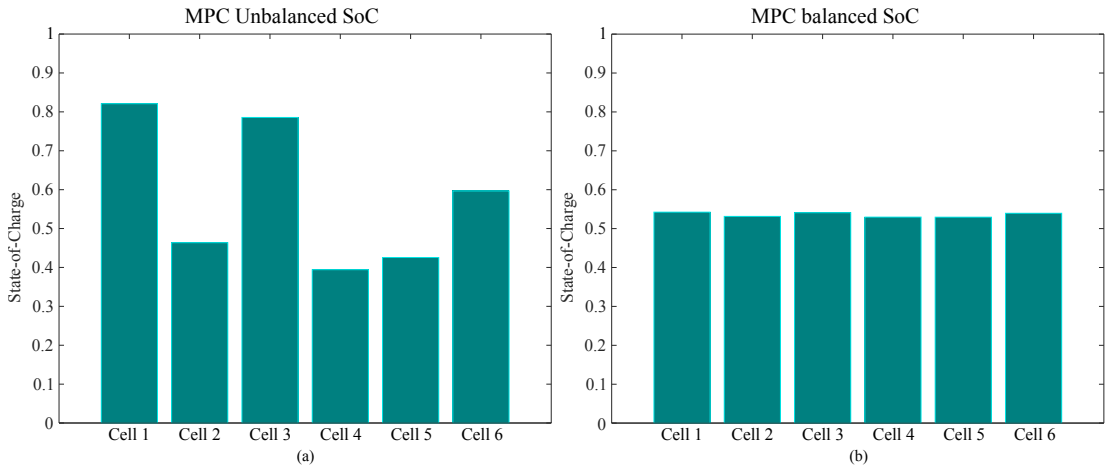

Figure 6.7: MPC Unbalanced(a); Balanced(b) State-of-Charge.

This shows the test ended with just a 1% difference in maximum and minimum SoC was achieved with 5mV in final voltages. According to the balance margin, LQR was able to successfully balance the cells state-of-charge. The balancing efficiency for the LQR method was calculated to be 0.61. The main issue with this type of control method is that battery balancing almost exclusively operates at the balancing limits. By constraining the balancing currents after getting an unconstrained solution does not give the best results i.e not minimum time with extra loss.

For the MPC experimental test, an initial set of start-of-charge values was

$$x_0 = [0.82,\ 0.46,\ 0.79,\ 0.39,\ 0.43,\ 0.60]$$

for cells 1 through 6 respectively. The initial voltage set (volts) for the same corresponding cells was

$$V_0 = \text{diag}[3.9098,\ 3.5991,\ 3.8724,\ 3.5575,\ 3.5764,\ 3.6991]$$

The test originally started with an arbitrary unbalance of 43% difference in maximum and minimum SoC and 351mV in starting voltages. At the end of balancing and after the predefined rest period, this system had a ending set of start-of-charge values equivalent to

$$x_\tau = [0.54,\ 0.53,\ 0.54,\ 0.53,\ 0.53,\ 0.54]$$

The final voltage set in volts was

$$V_0 = \text{diag}[3.6531,\ 3.6447,\ 3.6520,\ 3.6434,\ 3.6432,\ 3.6509]$$

This shows the test ended with just a 1% difference in maximum and minimum SoC was achieved with 9mV in final voltages. According to the balance margin, MPC was able to successfully balance the cells state-of-charge. The balancing efficiency for the MPC method was calculated to be the highest out of the three controllers at 0.71. This is because the intermediate cells have more constant current trajectories and is balanced in the minimum time as both the strongest and weakest cells are operated with the maximum link currents. A final remark about these results is that this shows a clear motivation behind adopting a MPC approach which is to apply more of a constant current that results in higher balancing efficiency and minimum time to balance.

Chapter 7

Conclusions

Many cells in a pack configured in both series and parallel orientations introduce monitoring and management difficulties. The capacity and the lifetime of the battery pack are determined by the weakest cell. Each cell must be properly monitored to prevent overcharge and over discharge of Lithium-ion cells. The differences in state-of-charge will cause further variations between each cell that only grow with time. To use the entire effective pack capacity, balancing the individual cells needs to occur. This thesis shows varies balancing topologies found in literature and implements a multiple transformer individual cell to stack topology for redistributive non-dissipative battery balancing. This was the chosen topology because in [5], the time to balance and energy dissipated remained constant as the number of cells increased.

Furthermore, three high level control strategies were designed to balance, i.e. equalize the state-of-charge of n number of series connected cells with m links. The control methods are rule based (RB) control, Linear Quadratic Regulator (LQR) control and Model Predictive Control (MPC). For comparison, a typical active dissipated topology using switched resistors [19, 38] was used with a rule based control

that drives the higher SoCs to the minimum SoC. If resistor values are chosen such that the current is small or less than 10mA/Ahr capacity, then each cell roughly can balance at a rate of 1% per hour [38]. However, if trying to employ the redistributive technique i.e operating all the time not just during charging then this technique could drain the entire battery pack in a few days [38]. Furthermore, it has a balancing efficiency of zero because the total initial unbalanced energy is lost i.e $E_U = E_L$.

The high level controllers are based on a general battery pack model that can be adopted for cells with different capacities since each cell is modeled by its capacity and state-of-charge. Also, it can be combined with various battery balancing topologies that are modeled by a topology matrix defined in [5] and the maximum current in each link. In practice, isolated DC/DC converters actuate the average balancing current defined by the high level controller. For the high level LQR controller, Linear transformations are used to transform the control into a regulation problem and to ensure that the control input is feasible. The main issue with this type of control method is that battery balancing almost exclusively operates at the balancing limits. By constraining the balancing currents after getting an unconstrained solution does not give the best results i.e not minimum time with extra loss. This result is validated by having a worse balancing efficiency than MPC of 0.61. The fast MPC controller is developed based on the minimum time to balance performance metric in [5]. The fast MPC controller applies the maximum input $\bar{u}$ if $\tau > T_s$. If $\tau \leq T_s$ then the input is scaled by a $\frac{\tau}{T_s}$ factor. The MPC approach is compared to a rule based strategy and shows that constant current will result in a single point of converge of the SoCs. This reduces any micro-cycles between charging and discharging of the intermediate battery cells [55] and improves the balancing efficiency.

Appendix

A Linear Quadratic Regulator MATLAB Script

```
%% Define Parameters
N = 6;                  % Number of cells
Cmax = 3.07*2;          % Nominal capacity for all cells (Ah)
Imax = 0.85;            % Maximum current through each link
Ts = 120;               % DSP Switching period
x0 = [0.1,0.2,0.3,0.4,0.5,0.6]';  %Example initial SoC Set
NL = N;                   % Number of links
T = ones(N)/N - eye(N); % Define network Topology matrix
Q = eye(N)*Cmax*3600; % Charge capacities
I = eye(NL)*Imax;     % Max Currents
B = [inv(Q)*T*I, -inv(Q)*T*I]; % B Matrix
B_ = inv(Q)*T*I;

%% Defining Constraints
Hup = [eye(NL);-eye(NL)];
Kup = [ones(NL,1);zeros(NL,1)];
Hum = [eye(NL);-eye(NL)];
Kum = [ones(NL,1);zeros(NL,1)];
Hu = [Hup,zeros(2*NL,NL);zeros(2*NL,NL),Hum];
Ku = [Kup;Kum];
go = [zeros(2*NL, 1); 1];

%% Transformation Matrix (L - differences between neighboring cells)
L = [eye(N-1),zeros(N-1,1)] + [zeros(N-1,1),-eye(N-1)];
H = go*go';
g = zeros(2*NL + 1,1);

%% Equality constraint
Heq = [zeros(1,NL),-zeros(1,NL)];
Keq = 0;

%% Linear Transformation
F = null(Heq);
u0 = pinv(Heq)*Keq;
H = Hu*F;
K = Ku - Hu*u0;

%% Regulation Problem
X_bar = L*x0;
B_bar = L*B*F;
zeroValueOffset = L*B*u0;

%% LQR Problem
A_bar = eye(N-1,N-1);
```

```
Q = 1e9*eye(N-1,N-1);
R = eye(2*N);
k_lqr = dlqr(A_bar, Ts*B_bar, Q, R); %Discrete LQR

%% SCRIPT Simulation
Nsim = 59;            %Number of k-time steps
tk = (0:Nsim-1);
xk = zeros(N,Nsim);
uk = zeros(N,Nsim);
tau_d = zeros(1,Nsim);
xk(:,1) = x0;

for i = 1 : Nsim-1
    %% LQR Control
    X_bar = L*xk(:,i);
    u_prime = k_lqr*X_bar;
    if min(u_prime) < 0
        u_prime = u_prime + abs(min(u_prime));
    end
    for id=1:length(K)
        if H(id,:)*u_prime > K(id)
            u_prime = u_prime *K(id)/(H(id,:)*u_prime);
        end
    end
    upm = F*u_prime + u0;
    uk(:,i) = upm(1:N) - upm(N+1:2*N);

    %% LQR Linear Battery Model
    xk(:,i+1) = xk(:,i) - Ts*B_*uk(:,i);
end

%% Plot State-of-Charge
figure(1);
plot(tk'*Ts/60, xk);

%% Plot Normalized Balancing Currents
figure(2);
plot(tk'*Ts/60, uk);
```

B Model Predictive Control MATLAB Script

```
    clc;
    clear all;
    close all;

    %% Define Parameters
N = 6;                  % Number of cells
Cmax = 3.07*2;          % Nominal capacity for all cells (Ah)
Imax = 0.85;            % Maximum current through each link
Ts = 120;               % DSP Switching period
x0 = [0.1,0.2,0.3,0.4,0.5,0.6]';  %Example initial SoC Set
NL = N;                   % Number of links
T = ones(N)/N - eye(N); % Define network Topology matrix
Q = eye(N)*Cmax*3600; % Charge capacities
I = eye(NL)*Imax;     % Max Currents
B = [inv(Q)*T*I, -inv(Q)*T*I]; % B Matrix
B_ = inv(Q)*T*I;

%% Defining Constraints
Hup = [eye(NL);-eye(NL)];
Kup = [ones(NL,1);zeros(NL,1)];
Hum = [eye(NL);-eye(NL)];
Kum = [ones(NL,1);zeros(NL,1)];
Hu = [Hup,zeros(2*NL,NL);zeros(2*NL,NL),Hum];
Ku = [Kup;Kum];
go = [zeros(2*NL, 1); 1];

%% Transformation Matrix (L - removes average SoC and leaves unbalanced SoC)
L = eye(N)-ones(N)/N;
H = go*go';
g = zeros(2*NL + 1,1);

%Constraints Formulated
Aineq = [Hu, -Ku; zeros(1,2*NL), -1];
bineq = [zeros(4*NL,1);0];
Aeq = [L*B, zeros(size(L*B,1),1)];

n__ = size(Aineq,2);
m__ = size(Aineq,1);
Hn = zeros(n__+m__);
Hn(1:n__,1:n__) = H;
gn = [g;zeros(m__,1)];
An = [Aeq,zeros(size(Aeq,1),m__);Aineq,eye(m__)];
bn = [-L*x0; bineq];
```

```
%% SCRIPT Simulation
Nsim = 59;            %Number of k-time steps
tk = (0:Nsim-1);
xk = zeros(N,Nsim);
uk = zeros(N,Nsim);
tau_d = zeros(1,Nsim);
xk(:,1) = x0;

for i = 1 : Nsim-1
    %% MPC Control
    bn = [-L*xk(:,i); bineq];
    % Substitute MPC_SOLVER with stnd solvers such as CPLEX & qpOASES
    [x_micro, exitflag] = MPC_SOLVER(Hn, gn, An, bn);

    %% Post Process x_micro
    tau_ = max(x_micro(2*N+1),1e-12);
    vpm = x_micro(1:2*N);
    if tau_ > Ts
        upm_out = vpm/tau_;
    else
        if tau_ > 0
            upm_out = vpm/Ts;
        else
            upm_out = zeros(2*6,1);
        end
    end
    u = (upm_out(1:N) -upm_out(N+1:2*N));

    %% MPC Linear Battery Model
    xk(:,i+1) = xk(:,i) + Ts*B_*uk(:,i);
end

%% Plot State-of-Charge
figure(1);
plot(tk'*Ts/60, xk);

%% Plot Normalized Balancing Currents
figure(2);
plot(tk'*Ts/60, uk);
```

C Rule Based MATLAB Script

```
clc;
clear all;
close all;

    %% Define Parameters
N = 6;                  % Number of cells
Cmax = 3.07*2;          % Nominal capacity for all cells (Ah)
Imax = 0.85;            % Maximum current through each link
Ts = 120;               % DSP Switching period
x0 = [0.1,0.2,0.3,0.4,0.5,0.6]';  %Example initial SoC Set
NL = N;                   % Number of links
T = ones(N)/N - eye(N); % Define network Topology matrix
Q = eye(N)*Cmax*3600; % Charge capacities
I = eye(NL)*Imax;      % Max Currents
B = [inv(Q)*T*I, -inv(Q)*T*I]; % B Matrix
B_ = inv(Q)*T*I;
L = eye(N)-ones(N)/N;

%% SCRIPT Simulation
Nsim = 59;              %Number of k-time steps
tk = (0:Nsim-1);
xk = zeros(N,Nsim);
uk = zeros(N,Nsim);
tau_d = zeros(1,Nsim);
xk(:,1) = x0;

for i = 1 : Nsim-1
    %% Rule based control
    soc_average = sum(xk(:,i))/N;
    tdL = norm(L*xk(:,i),1);
    for iL = 1:N
        if(tdL > 0.005)
            if (xk(iL,i) >= soc_average )
                % If above average, discharge.
                upm1(iL) = 1;
                upm2(iL) = 0;
            elseif (xk(iL,i) < soc_average )
                %  If below average, charge.
                upm1(iL) = 0;
                upm2(iL) = -1;
            end
        end
        uk(iL,i) = upm1(iL) + upm2(iL);
    end
```

```
    % Linear Plant Model
    xk(:,i+1) = xk(:,i) + Ts*B_*uk(:,i);
end

%% Plot State-of-Charge
figure(1);
plot(tk'*Ts/60, xk);

%% Plot Normalized Balancing Currents
figure(2);
plot(tk'*Ts/60, uk);
```

Bibliography

[1] B. Bilgin, P. Magne, P. Malysz, Y. Yang, V. Pantelic, M. Preindl, A. Korobkine, W. Jiang, M. Lawford, and A. Emadi, "Making the Case for Electrified Transportation," *IEEE Transactions on Transportation Electrification*, vol. 1, no. 1, pp. 4–17, 2015.

[2] The Boston Consulting Group, "Batteries for Electric Cars - Challenges, Opportunities, and the Outlook to 2020," Tech. Rep. 1, 2010.

[3] Panasonic, "Panasonic NCR18650A Datasheet," Tech. Rep., 2012.

[4] D. Andrea, *Battery Management Systems for Large Lithium-ion Battery Packs*. Artech House, 2010.

[5] M. Preindl, C. Danielson, and F. Borrelli, "Performance evaluation of battery balancing hardware," in *European Control Conference*, jul 2013, pp. 4065–4070.

[6] A. Saliva, "Design Guide for Off-line Fixed Frequency DCM Flyback Converter," Infineon, Tech. Rep. January, 2013.

[7] LTC, "Linear Technology - LTC DC2100A Demoboard: User Manual," Tech. Rep., 2013.

[8] ——, "Linear Technology - LTC3300-1: High Efficiency Bidirectional Multicell Battery Balancer (Datasheet)," Tech. Rep., 2013.

[9] *International Technology Perspectives 2008 - Scenarios and strategies to 2050.* International Energy Agency, 2008.

[10] E. Chemali, M. Peindl, P. Malysz, and A. Emadi, "Electrochemical and Electrostatic Energy Storage and Management Systems for Electric Drive Vehicles: State-of-the-Art Review and Future Trends," *IEEE Journal of Emerging and Selected Topics in Power Electronics*, vol. 6777, no. c, pp. 1–1, 2016.

[11] N. Rauh, T. Franke, and J. F. Krems, "Understanding the Impact of Electric Vehicle Driving Experience on Range Anxiety," *Human Factors: The Journal of the Human Factors and Ergonomics Society*, vol. 57, no. 1, pp. 177–187, 2015.

[12] O. Veneri, L. Ferraro, C. Capasso, and D. Iannuzzi, "Charging infrastructures for EV: Overview of technologies and issues," *Electrical Systems for Aircraft, Railway and Ship Propulsion, ESARS*, pp. 0–5, 2012.

[13] California Environmental Protection Agency Air Resources Board, "Technology Assessment: Medium- and Heavy- Duty Battery Electric Trucks and Buses," Tech. Rep. October 2015 (Draft), 2015.

[14] S. Abu-Sharkh and D. Doerffel, "Rapid test and non-linear model characterisation of solid-state lithium-ion batteries," *Journal of Power Sources*, vol. 130, no. 1-2, pp. 266–274, 2004.

[15] N. H. Kutkut, H. L. N. Wiegman, D. M. Divan, and D. W. Novotny, "Charge equalization for an electric vehicle battery system," *IEEE Transactions on Aerospace and Electronic Systems*, vol. 34, no. 1, pp. 235–246, 1998.

[16] B. Lindemark, "Individual cell voltage equalizers (ICE) for reliable battery performance," in *Energy Conference*, vol. 91, 1991, pp. 196–201.

[17] C. S. Moo, Y. C. Hsieh, and I. S. Tsai, "Charge equalization for series-connected batteries," *IEEE Transactions on Aerospace and Electronic Systems*, vol. 39, no. 2, pp. 704–710, 2003.

[18] N. H. Kutkut and D. M. Divan, "Dynamic equalization techniques for series battery stacks," in *International Telecommunications Energy Conference*, 1996, pp. 514–521.

[19] J. Cao, N. Schofield, and A. Emadi, "Battery balancing methods: A comprehensive review," in *IEEE Vehicle Power and Propulsion Conference*, 2008, pp. 3–8.

[20] R. Lache, D. Galves, and P. Nolan, "Electric cars: Plugged in 2," Tech. Rep. November, 2009.

[21] D. H. Zhang, S. Qiu, G. R. Zhu, and W. Chen, "Balancing Control Strategy for Li-ion Batteries String Based on Dynamic Balanced Point," in *IEEE Vehicle Power and Propulsion Conference*, no. 2011, 2013, pp. 60–64.

[22] N. Omar, M. Daowd, P. van den Bossche, O. Hegazy, J. Smekens, T. Coosemans, and J. van Mierlo, "Rechargeable energy storage systems for plug-in hybrid electric vehicles-assessment of electrical characteristics," *Energies*, vol. 5, no. 8, pp. 2952–2988, 2012.

[23] McMaster University, "MechEng739: Management and Control of Electric Vehicle Batteries," 2015.

[24] B. Xiao and Y. Shi, "A universal state-of-charge algorithm for batteries," in *Design Automation Conference*, 2010, pp. 687–692.

[25] G. L. Plett, "Extended Kalman filtering for battery management systems of LiPB-based HEV battery packs. Part 1: Background," *Journal of Power Sources*, vol. 161, no. 2, pp. 1356–1368, 2004.

[26] M. Charkhgard and M. Farrokhi, "State-of-charge estimation for lithium-ion batteries using neural networks and EKF," *IEEE Transactions on Industrial Electronics*, vol. 57, no. 12, pp. 4178–4187, 2010.

[27] D. Howey, P. Mitcheson, V. Yufit, G. Offer, and N. Brandon, "Online measurement of battery impedance using motor controller excitation," *IEEE Transactions on Vehicular Technology*, vol. 63, no. 6, pp. 2557–2566, 2014.

[28] R. Feng, S. Zhao, and X. Lu, "On-line estimation of Dynamic State-of-Charge for lead acid battery based on fuzzy logic," in *International Conference on Measurement, Information and Control*, no. 1, 2013, pp. 447–451.

[29] R. Ling, Y. Dong, H. Yan, M. Wu, and Y. Chai, "Fuzzy-PI control battery equalization for series connected lithium-ion battery strings," in *Electronics and Motion Control Conference (IPEMC)*, vol. 4, no. 5, 2012, pp. 2631–2635.

[30] K. Young, C. Wang, L. Y. Wang, and K. Strunz, *Electric Vehicle Integration into Modern Power Networks*, 2013.

[31] S. M. Lukic, J. Cao, R. C. Bansal, F. Rodriguez, and A. Emadi, "Energy storage systems for automotive applications," *IEEE Transactions on Industrial Electronics*, vol. 55, no. 6, pp. 2258–2267, 2008.

[32] A. Affanni, A. Bellini, G. Franceschini, P. Guglielmi, and C. Tassoni, "Battery choice and management for new-generation electric vehicles," *IEEE Transactions on Industrial Electronics*, vol. 52, no. 5, pp. 1343–1349, 2005.

[33] M. J. Isaacson, R. P. Hollandsworth, P. J. Giampaoli, F. A. Linkowsky, A. Salim, and V. L. Teofil, "Advanced Lithium Ion Battery Charger," in *Fifteenth Annu. Battery Conf. Applications and Advances*, 2000, pp. 798–801.

[34] G. Mulder, N. Omar, S. Pauwels, M. Meeus, F. Leemans, B. Verbrugge, W. De Nijs, P. Van Den Bossche, D. Six, and J. Van Mierlo, "Comparison of commercial battery cells in relation to material properties," *Electrochimica Acta*, vol. 87, pp. 473–488, 2013.

[35] H. Popp, J. Attia, F. Delcorso, and A. Trifonova, "Lifetime analysis of four different lithium ion batteries for (plugin) electric vehicle," *Transport Research Arena*, 2014.

[36] H. Chen, T. N. Cong, W. Yang, C. Tan, Y. Li, and Y. Ding, "Progress in electrical energy storage system: A critical review," *Progress in Natural Science*, vol. 19, no. 3, pp. 291–312, 2009.

[37] L. Mccurlie, M. Preindl, P. Malysz, and A. Emadi, "Simplified Control for Redistributive Balancing Systems using Bidirectional Flyback Converters," in *IEEE Transportation Electrification Conference and Exposition*, 2015.

[38] S. Moore and P. Schneider, "A Review of Cell Equalization Methods for Lithium Ion and Lithium Polymer Battery Systems," *SAE World Congress*, pp. Doc. 2001–01–0959, 2001.

[39] B. Lawson, "A Software Configurable Battery," *EVS26 International Battery, Hybrid and Fuel Cell Electric Vehicle Symposium, Los Angeles, California*, 2012.

[40] N. H. Kutkut, "A Modular Non Dissipative Current Diverter For Ev Battery Charge Equalization," in *Applied Power Electronics Conference and Exposition*, 1998, pp. 686–690.

[41] M. Daowd, N. Omar, P. van den Bossche, and J. van Mierlo, "A review of passive and active battery balancing based on MATLAB/Simulink," *International Review of Electrical Engineering*, vol. 6, no. 7, pp. 2974–2989, 2011.

[42] R. Erickson, "The Flyback Converter - Lecture notes ECEN4517," 2012.

[43] Y. Barksukov and J. Qian, *Battery Power Management for Portable Devices*, 2013.

[44] M. Caspar and S. Hohmann, "Optimal Cell Balancing with Model-based Cascade Control by Duty Cycle Adaption," *The International Federation of Automatic Control*, pp. 10 311–10 318, 2014.

[45] E. D. Sontag, "An algebraic approach to bounded controllability of linear systems," *International Journal of Control*, vol. 39, no. 1, pp. 181–188, 1984.

[46] J. Choi, "On the stabilization of linear discrete time systems subject to input saturation," *Systems & Control Letters*, vol. 36, 1999.

[47] T. Hofman, M. Steinbuch, R. M. V. Druten, and a. F. a. Serrarens, "Rule-Based Equivalent Fuel Consumption Minimization Strategies for Hybrid Vehicles," *IFAC Symposium on Mechatronic Systems*, vol. 17, no. 1, 2008.

[48] S. Malkhandi, "Fuzzy logic-based learning system and estimation of state-of-charge of lead-acid battery," *Engineering Applications of Artificial Intelligence*, vol. 19, no. 5, pp. 479–485, 2006.

[49] M. Sorrentino, G. Rizzo, and I. Arsie, "Analysis of a rule-based control strategy for on-board energy management of series hybrid vehicles," *Control Engineering Practice*, vol. 19, no. 12, pp. 1433–1441, 2011.

[50] LTC, "Linear Technology - DC2100A: Bi-Directional Cell Balancer," Tech. Rep.

[51] A. M. Imtiaz and F. H. Khan, ""Time shared flyback converter" based regenerative cell balancing technique for series connected li-ion battery strings," *IEEE Transactions on Power Electronics*, vol. 28, no. 12, pp. 5960–5975, 2013.

[52] S. A. Akbarabadi, H. Atighechi, and J. Jatskevich, "Corrected state-space averaged-value modeling of second-order flyback converter including conduction

losses," in *IEEE Canadian Conference of Electrical and Computer Engineering*, 2013.

[53] Y. Yuanmao, K. W. E. Cheng, and Y. P. B. Yeung, "Zero-current switching switched-capacitor zero-voltage-gap automatic equalization system for series battery string," *IEEE Transactions on Power Electronics*, vol. 27, no. 7, pp. 3234–3242, 2012.

[54] H. He, R. Xiong, and J. Fan, "Evaluation of Lithium-Ion Battery Equivalent Circuit Models for State of Charge Estimation by an Experimental Approach," *Energies*, vol. 4, no. 12, pp. 582–598, 2011.

[55] E. Chemali, L. Mccurlie, B. Howey, T. Stiene, M. M. Rahman, M. Preindl, R. Ahmed, and A. Emadi, "Minimizing Battery Wear in a Battery-Ultracapacitor Hybrid Energy Storage System using a Linear Quadratic Regulator," in *IEEE IECON*, 2015, pp. 3265–3270.